Adiabatic Spectroscopy and a Variational Quantum Adiabatic Algorithm

Benjamin F. Schiffer,[1,2,*] Jordi Tura,[1,2,3] and J. Ignacio Cirac[1,2]

[1] *Max-Planck-Institut für Quantenoptik, Hans-Kopfermann-Str. 1, Garching D-85748, Germany*

[2] *Munich Center for Quantum Science and Technology (MCQST), Schellingstr. 4, Munich D-80799, Germany*

[3] *Instituut-Lorentz, Universiteit Leiden, P.O. Box 9506, Leiden 2300 RA, Netherlands*

(Received 3 May 2021; accepted 7 April 2022; published 6 June 2022)

Preparation of the ground state of a Hamiltonian is a problem of great significance in physics, with deep implications in the field of combinatorial optimization. The adiabatic algorithm is known to return the ground state for sufficiently long preparation times that depend on the *a priori* unknown spectral gap. Our work relates in a twofold way. First, we propose a method to obtain information about the spectral profile of the adiabatic evolution. Second, we present the concept of a variational quantum adiabatic algorithm (VQAA) for optimized adiabatic paths. We aim at combining the strengths of the adiabatic and the variational approaches for fast and high-fidelity ground-state preparation while keeping the number of measurements as low as possible. Our algorithms build upon ancilla protocols that we present, which allow us to directly evaluate the ground-state overlap. We benchmark for a nonintegrable spin-1/2 transverse and longitudinal Ising chain with $N = 53$ sites using tensor-network techniques. Using a black-box gradient-based approach, we report a reduction in the total evolution time for a given desired ground-state fidelity by a factor of 10, which makes our method suitable for the limited decoherence time of noisy-intermediate scale quantum devices.

DOI: 10.1103/PRXQuantum.3.020347

I. INTRODUCTION

Remarkable scientific progress in recent years has led to the first noisy intermediate-scale quantum (NISQ) [1] devices. Current NISQ devices are still limited by the number of qubits available, their gate fidelity, and the maximum circuit depth. Much research effort is put into the investigation of algorithms for digital NISQ devices that could hold the promise of a (practical) quantum advantage [2,3]. Nevertheless, the simulation of large quantum many-body systems on these devices will still remain challenging over the coming years. Analog quantum simulators, however, are able to implement some quantum dynamics very efficiently. Furthermore, analog quantum simulators are especially well suited for probing universal features of quantum many-body systems. Several powerful concepts and experimental realizations of digital NISQ devices and analog quantum simulators have been put forward [4–6].

One particularly important problem is to prepare the ground state of quantum many-body systems, this being relevant for a wide range of physics applications and closely related to combinatorial optimization tasks. Quantum computers already save an exponential memory cost compared to a classical computer in the representation of the quantum state, making a quantum device the natural choice to compute desired quantum states. Moreover, ground states are also of great importance for optimization problems, as the solutions to combinatorial problems can be naturally encoded into a classical Hamiltonian.

The problem of finding the ground state is known to be quantum Merlin-Arthur (QMA) complete [7], which translates roughly to the analog of nondeterministic polynomial (NP) complete for a quantum computer. However, two different promising heuristic approaches have been established. First and most straightforwardly, there is the adiabatic approach. In order to prepare the ground state of a target Hamiltonian H_T with a quantum adiabatic algorithm (QAA) [8], one takes an adiabatic path $H(s) = (1-s)H_0 + sH_T$. Starting from the ground state of a trivial Hamiltonian H_0 at $s(0) = 0$, the parameter $s(t)$ is changed with time up to the final value $s(T) = 1$. Given a nondegenerate ground state along the path, the adiabatic algorithm is known to return the ground state for a sufficiently long preparation time T. However, T is a function of the spectral energy gap $\Delta(s)$ between the ground state and the first excited state along the adiabatic path and is not known *a priori* [9–12]. Due to the limited decoherence times of

*Benjamin.Schiffer@mpq.mpg.de

current NISQ devices and analog quantum simulators, the preparation time T is of great relevance for the feasibility of the adiabatic approach. Different adiabatic paths can be constructed and a linear time schedule is generally not optimal in the sense of a minimal T. This is especially relevant when the gap $\Delta(s)$ becomes very small, as it occurs in the presence of a quantum phase transition.

Optimal adiabatic paths have been the subject of intensive research efforts both in the framework of shortcuts to adiabaticity as well as optimal control theory [13,14]. For the problem of an unstructured search, Grover-type speed-ups have been shown, where the full spectral information about the problem is available [15,16].

Another approach to preparation of the ground state is the quantum approximate optimization algorithm (QAOA) [17], which seeks to overcome the limitations of the QAA. It generalizes the QAA by splitting the total time into chunks, $\{T_i\}$, where one alternates between H_0 and H_T, and takes $\{T_i\}$ as the variational parameters. The QAOA includes the QAA in the sense that there exist $T_i = iT/L$, where $i = \{1, \ldots, L\}$ and L is sufficiently large, corresponding to the Trotter evolution of the QAA. However, it is expected that the QAOA can provide a speed-up by choosing the parameters $\{T_i\}$ larger than in Trotterized QAA.

In fact, the QAOA belongs to a wider class of variational quantum algorithms (VQA) in the spirit of the variational principle, which is widely used in physics. While the quantum computer is used to prepare the states and perform the measurements, the optimization of the parameters is carried out classically. In practice, the performance of the VQA can be curbed, since the number of measurements necessary to estimate an objective function may scale unfavorably, and due to the presence of plateaus in the energy landscape, including noise-induced barren plateaus [18–21].

In this work, we propose the concept of a variational quantum adiabatic algorithm (VQAA) to find optimal adiabatic paths for high-fidelity ground-state preparation, thereby combining the strengths of adiabatic state preparation and the VQA. Akin to the QAOA, the times $\{T_i\}$ are treated as the variational parameters. However, the evolution in the different chunks is performed adiabatically, similarly to the QAA. Here, the VQAA differs from the fixed Hamiltonians found in the QAOA. The VQAA allows for a significant acceleration compared to the QAA with a linear adiabatic path and yet requires fewer parameters and measurements than the QAOA.

We discuss different approaches to finding such a parametrized optimal adiabatic path. The approaches are suited to different resource requirements, some making use of ancilla protocols to estimate the ground-state overlap. These protocols rely on controlled unitary evolution, which leads to many benefits in the quantum computing setting. Besides being central to the canonical quantum phase-estimation algorithm [22], it also allows us to access overlaps between initial and final states for a given unitary transformation by looking at the ancilla only and it enables spectral projections on the state of the system if one enables postselection on the ancilla [23].

The ancilla techniques presented here may prove to be useful tools by themselves for other variational algorithms. This is especially true for our protocol with two ancilla qubits, as this constitutes a case of nontrivial distributed quantum computing. The interconnection of multiple quantum devices using a coherent link is a promising path forward for the field of quantum computing [24].

We benchmark the different algorithms with a quantum Hamiltonian and up to $N = 100$ qubits, which is what is expected for the new generation of NISQ devices or analog quantum simulators. We take a Hamiltonian that is nontrivial (nonintegrable) but for which we can simulate the action of a quantum computer classically using tensor-network techniques. In the case of a small gap in the adiabatic path, in the presence of a phase transition, we report significant reductions in the required evolution time to reach a given desired ground-state fidelity. For a chain of $N = 53$ qubits and a target fidelity of 90%, the VQAA is able to reduce the total evolution time by a factor of 10 compared to a linear adiabatic path.

Having mentioned earlier that the spectral gap $\Delta(s)$ is *a priori* unknown, obtaining knowledge about the spectral gap $\Delta(s)$ can be as hard a problem as finding the ground state itself. However, due to the interconnection between the spectral gap and the performance of adiabatic state preparation, we are able to propose a form of adiabatic spectroscopy to find spectral-gap properties. By performing adiabatic sweeps on the system and being equipped with either the ancilla protocols for ground-state estimation or backward time evolution, a measure for both the position and the smallness of the spectral gap can be obtained. A related scheme using backward time evolution, albeit initializing the evolution in a superposition, has been suggested in Ref. [25]. Knowledge about the spectral gap may be applied to gain important insights about quantum many-body physics, obtain the phase diagram of a physical system, or formulate the optimal path for adiabatic state preparation.

The structure of this paper is as follows. In Sec. II, we outline our main results. Then, we discuss our approach to adiabatic spectroscopy in Sec. III, and in Sec. IV we present two protocols for estimating the ground state at a given point along the adiabatic path using one or two ancillas. In Sec. V, we introduce the general concept of a VQAA for ground-state preparation and discuss different specific algorithms with different resource requirements (Sec. VI). After that, in Sec. VII, the model for benchmarking our algorithms is described and we present our results. Finally, we comment on the number of measurements necessary in our approach (Sec. VII D) and the

impact of noise on our algorithms (Sec. VIII). In the appendices, we give the necessary background to make the paper self-contained: a theoretical description of the adiabatic algorithm and the QAOA as well as Bayesian inference for beta-Bernoulli models, which are relevant for performing hypothesis testing.

II. MAIN RESULTS

Our main results include (1) protocols for eigenstate-closeness estimation and (2) a proposal for adiabatic spectroscopy, as well as (3) a concept for VQAAs, including a black-box gradient-based method:

(1) Given the possibility of implementing controlled unitary evolution on a quantum state, where the dynamics are controlled by a single ancilla qubit, information about the closeness to the next eigenstate can be extracted from the ancilla. We show that for a quantum state $|\psi\rangle = \sum_j \psi_j |\phi_j\rangle$ and Hamiltonian $H = \sum_j E_j |\phi_j\rangle\langle\phi_j|$, we need to obtain $\alpha := \sum_j |\psi_j|^2 \exp(-iE_j\tau)$ by measuring the ancilla. Then, for suitable τ, we can deduce that the state $|\psi\rangle$ is an eigenstate of H only if $|\alpha| = 1$. By a self-consistent argument and suitable construction, the closest eigenstate may be identified with the ground state.

(2) The profile of the spectral gap $\Delta(s)$ between the ground-state and the first excited-state energy of an interpolating Hamiltonian $H(s)$ is closely connected to the evolution time T required for adiabatic state preparation. We analyze the evolution time $T(s)$ necessary to prepare the ground state of $H(s)$ with a given target fidelity. The ground-state fidelity is computed either by time evolving both forward and backward and measuring the fidelity with the initial product state or by making use of the ancilla protocol, which is generally expected to give superior results. After obtaining the data points for $T(s)$, we interpolate the curve and compute the derivative. Corresponding to physical intuition, the curve of the evolution time features a strong increase when a small gap is crossed. The derivative $\partial T/\partial s$ can then provide the position and also a measure for the smallness of the spectral gap (Fig. 1).

(3) In our work, we present the concept of the VQAA and give specific algorithms that attempt to improve over the QAA. The main idea is to optimize the adiabatic path $s(t)$ by performing a moderate number of measurements. In our setup, $s(t)$ depends on a set of parameters, which are chosen through optimization procedures. The key ingredient is to use the overlap with the ground state as the figure of merit. The algorithms presented in this work make use of different protocols to estimate this overlap and are also distinguished in the way the optimization is performed: either by intending to remain in the ground state at intermediate steps in the adiabatic path or by optimizing for a maximum ground-state overlap at the end of the state preparation (as in the QAOA). The main feature of the method presented in this paper is that it requires fewer measurements. Our approach is well suited to be used in NISQ devices or analog quantum simulators by reducing the required preparation time and thus avoiding decoherence. Without knowing the adiabatic spectrum beforehand, the optimal adiabatic paths yield the desired ground state with high fidelity at only a fraction of the total evolution time of a nonoptimized adiabatic algorithm (Fig. 2).

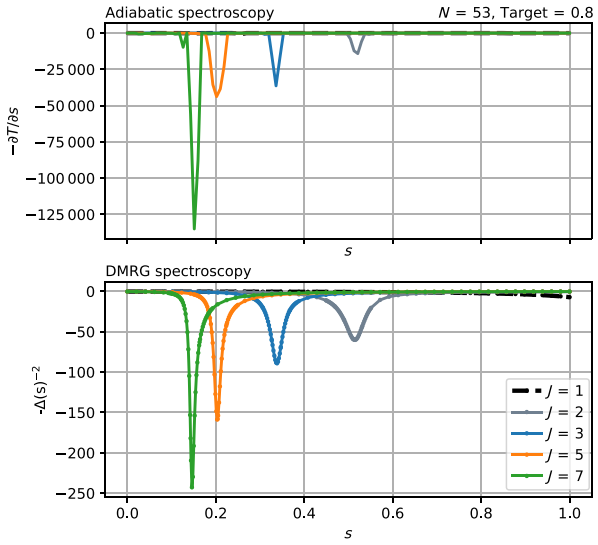

FIG. 1. Adiabatic spectroscopy for a chain of $N = 53$ qubits and a target ground-state fidelity of 0.7. For the Hamiltonian $H(J,g,h) = \sum_i (J\sigma_i^z\sigma_{i+1}^z + h\sigma_i^x + g\sigma_i^z)$, the adiabatic path is a linear interpolation from $H(0,1,0)$ to $H(J,1,1)$. The minima of the different curves correspond to the position and smallness of the respective spectral gaps. In the lower plot, $-\Delta(s)^{-2}$, obtained using density-matrix-renormalization-group (DMRG) methods, is shown as a comparison. The match with the Landau-Zener scaling is not exact, as higher-order corrections from adiabatic perturbation theory play a role.

III. ADIABATIC SPECTROSCOPY

We seek to gain insights about the adiabatic spectrum of the Hamiltonian

$$H(s) = (1-s)H_0 + sH_T. \tag{1}$$

The Hamiltonian $H(s)$ describes the adiabatic evolution from the ground state of a trivial Hamiltonian H_0 at $s = 0$ to the ground state of H_T at $s = 1$, where $s = t/T$ is the

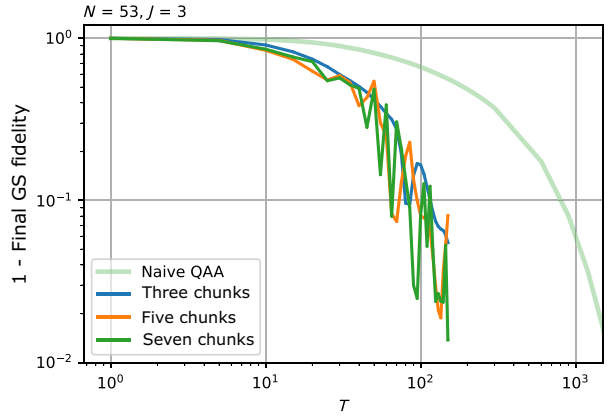

FIG. 2. Black-box VQAA results for 53 qubits and the ZZXZ model for the case of a crossed phase transition ($J = 3$). Results for three, five, and seven chunks, respectively, are shown. More chunks do not improve the results as for one avoided level crossing an optimized path can already be approximated with very few chunks. The quantum-classical feedback loop converges to optimized adiabatic paths that prepare the ground state with $> 90\%$ fidelity for $T \lesssim 100$. In order to achieve this ground-state fidelity with (nonoptimized) naive QAA, an evolution time about 10 times larger would be required.

parametrized time. The probability that the system transitions out of the ground state in the course of the evolution is intimately connected with the size of the spectral gap $\Delta(s) = E_1(s) - E_0(s)$ between the ground-state and the first excited-state energy. For each s_i in a set of data points $\{s_i\}$, $i \in \{1, \ldots, r\}$, in which r is the resolution of the spectroscopy, an efficient root-finding algorithm is used (e.g., using a bisection algorithm on the time variable T_i) to find the evolution time T_i, which reaches a given target ground-state overlap O_T (for a simple algorithmic description, see the Supplemental Material [26]).

If a small gap is crossed in the adiabatic path—e.g., at s^*—this will correspond to a large increase of $\{T_i\}$ around and beyond the value s^*. Hence, if we observe such a rise in the required evolution times $\{T_i\}$, we conclude that a local minimum in the spectral gap $\Delta(s^*)$ must be present. In this manner, the position of a small spectral gap can be obtained. Moreover, the smallness of $\Delta(s^*)$ is related to the steepness of the increase in the $\{T_i\}$ around s^*. For the Landau-Zener (LZ) model, we establish the relation $\partial T(s)/\partial s \sim 1/\Delta(s)^2$ around the minimal gap (Appendix A). Since the LZ approach is a toy model to qualitatively study the property of the spectral gap in adiabatic algorithms, we presume that a similar scaling could persist in a more general sense.

In order to obtain a measure for the ground-state overlap for given s_i, we propose two different approaches. The first approach is to not make use of the ancilla protocol and is thus very simple to implement. The initial ground state $|\psi_0\rangle$ at $s = 0$ is adiabatically time evolved forward with evolution time $\widetilde{T}_j$, implemented by the unitary operator $U_{0\to s_i}(\widetilde{T}_j)$. Here, the $\widetilde{T}_j$ denote the probing values in the search. We seek to determine the forward time so that we obtain the evolution time T_i that succeeds in reaching the given overlap O_T. Next, the interactions are reversed in a backward time evolution from $s = s_i$ to $s = 0$ implemented by $U_{0\leftarrow s_i}(\widetilde{T}_j^{\mathcal{B}})$. The backward time $\widetilde{T}_j^{\mathcal{B}} \gg \widetilde{T}_j$ is chosen to be larger than the forward time evolution. This allows for a trivial measurement of the ground-state overlap at $s = 0$,

$$\widetilde{O}_j = \left|\langle\psi_0|U_{0\leftarrow s_i}(\widetilde{T}_j^{\mathcal{B}})U_{0\to s_i}(\widetilde{T}_j)|\psi_0\rangle\right|, \tag{2}$$

as the state $|\psi_0\rangle$ is a product state. Once a $\widetilde{T}_j$ is found for which $\widetilde{O}_j \approx O_T$, we set $T_i := \widetilde{T}_j$ and proceed with the next data point s_{i+1}. Note that it is also sensible to use a large constant evolution time for the backward path.

We extend this approach by noting that if a small spectral gap $\Delta(s^*)$ is found and we continue to probe for those s_i for which $s_i > s^*$, it is economical to make use of the spectral information already obtained. In the spirit of the VQAA, the adiabatic schedule used in the spectroscopy should be altered so that the evolution around s^* is performed very slowly. In this manner, multiple gaps in the adiabatic spectrum could be investigated. This ancilla-free approach provides the least stringent requirements on the experimental setup in a NISQ framework.

However, with some additional effort, it is possible to directly estimate the ground-state overlap without going back to the initial state at $s = 0$. This second approach hinges on the ability to obtain a measure for the eigenstate closeness through an ancilla protocol. For every data point in $\{s_i\}$, we obtain the ground-state overlap for different $\widetilde{T}_j$ directly:

$$\widetilde{O}'_j = \left|\langle \mathrm{GS}_{s_i}|U_{0\to s_i}(\widetilde{T}_j)|\psi_0\rangle\right|, \tag{3}$$

where $|\mathrm{GS}_{s_i}\rangle$ is the ground state at s_i. Now, just as in the first approach, we search for the $\widetilde{T}_j$ such that $\widetilde{O}'_j \approx O_T$ and set $T_i := \widetilde{T}_j$.

Hence, this form of adiabatic spectroscopy can provide a tool in order to experimentally gain knowledge about the adiabatic spectrum. We simulate this technique classically with $N = 53$ qubits for different spectral profiles and present the results in Fig. 1 and Sec. VII B.

IV. PROTOCOL FOR GROUND-STATE CLOSENESS ESTIMATION

A very important ingredient of our algorithms is the ability to estimate the overlap with a nondegenerate ground state. In this section, we introduce two suitable protocols using ancillas and comment briefly on their benefits. The ancilla protocols only require the ability to implement unitary evolution controlled on a single ancilla and to perform

measurements on the ancilla. Controlled unitary evolution is a valuable ingredient for quantum computing, e.g., in the well-known quantum phase-estimation algorithm [22]. The use of ancilla measurements for ground-state preparation has been investigated previously and can be used to construct spectral projection operators similar to the quantum Zeno effect if one allows for postselection on the ancilla [23]. In our work, we utilize the ancilla in order to extract information about the eigenstate closeness, which can then be used in the different applications of the VQAA in a highly versatile manner.

A. Single-ancilla protocol

We first present a protocol for eigenstate-closeness estimation using a single ancilla in the $|+\rangle$ state [27]. The quantum circuit shown in Fig. 3 can be used to compare the overlap of an initial quantum state $|\psi\rangle$ with the state after the unitary evolution $|\psi_{\text{evo}}\rangle$:

$$\langle\psi|\psi_{\text{evo}}\rangle = \langle\sigma_x + i\sigma_y\rangle_{\text{ancilla}}\,. \tag{4}$$

For a fixed Hamiltonian $H = \sum_j E_j\,|\phi_j\rangle\,\langle\phi_j|$ with the unitary

$$U|\phi_j\rangle = e^{-iH\tau}\,|\phi_j\rangle = e^{-iE_j\tau}\,|\phi_j\rangle\,, \tag{5}$$

we write the normalized state $|\psi\rangle = \sum_j \psi_j\,|\phi_j\rangle$ in the eigenbasis of H. Then, we analyze the quantum circuit for this choice of U. We obtain, for the density matrix of the ancilla qubit after the controlled unitary evolution (Appendix B 1),

$$\rho_a = \sum_j \frac{|\psi_j|^2}{2}\begin{pmatrix} 1 & e^{iE_j\tau} \\ e^{-iE_j\tau} & 1 \end{pmatrix}. \tag{6}$$

For a quantum state $|\psi\rangle$ that is an eigenstate, the rank of ρ_a will be 1. Due to the specific structure of ρ_a, only one off-diagonal matrix element is needed in order to determine the rank of ρ_a. We note, using Eq. (B8), that

$$\langle\psi|\psi_{\text{evo}}\rangle = \sum_j |\psi_j|^2 e^{-iE_j\tau} =: \alpha. \tag{7}$$

For suitable τ, $|\psi_{\text{evo}}\rangle$ is an eigenstate only if $|\alpha| = 1$. The time τ needs to be chosen so that the complex summands of α with nonvanishing amplitude do not have

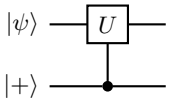

FIG. 3. The quantum circuit for unitary dynamics controlled by a single ancilla qubit in the $|+\rangle$ state.

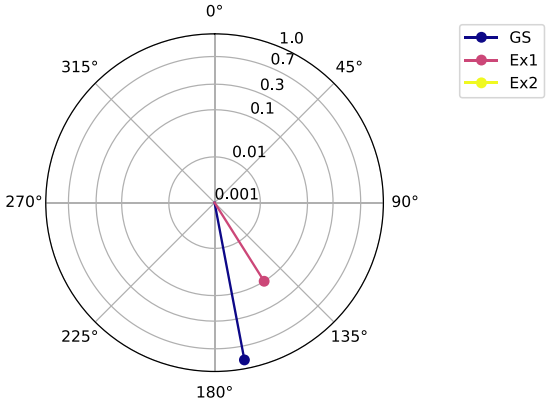

FIG. 4. An exemplary eigenstate clock featuring the complex summands of α for τ=1. Here, the term corresponding to the ground state $|\psi_0|^2\exp(-iE_0\tau)$ and the first excited-state term $|\psi_1|^2\exp(-iE_1\tau)$ lie quite closely together in phase, which leads to problematic constructive interference. However, as the pointers rotate with their respective eigenenergies, they will be well separated for suitable larger τ. Note that in this instance, the summands corresponding to higher excited eigenstates are taken to be very small and are not visible.

approximately equal phases. In this unlikely case of matching phases, we would see constructive interference, so that $|\alpha| = 1$ could be true even if $|\psi_{\text{evo}}\rangle$ is not an eigenstate. Visualizing the summands of α on a complex plane (Fig. 4), this becomes rather intuitive. The choice for τ is related to the spectrum of H. For the sake of this argument, we assume that the overlaps with the ground state and the first excited state are the only other nonvanishing overlaps. Then, an arbitrary τ would correspond to choosing an $l \in \mathbb{Z}$ in $\tau = \pi l/\Delta$ at random (Appendix B 3). For $l \gg 1$, the probability of choosing an odd value of l is approximately 1/2. Therefore, by testing several random values of $\tau \in O(\Delta^{-1})$ it is possible to deduce information about the system whether it is in a mixed state or an eigenstate with high confidence (cf. the Chernoff-Hoeffding bound in Sec. VII D). Through a self-consistent argument, we can conclude that the main contribution to α comes from the ground state, provided that we remain nearly adiabatic throughout the path. We can bound the maximal error in $|\alpha(\tau)|^2$ by computing the average for up to large values of an uniformly distributed τ as

$$E^2 := \lim_{K\to\infty} \mathbb{E}_{\tau\,\sim\,\text{unif. dist. in }[0,K]}(|\alpha(\tau)|^2) = \sum_i |\psi_i|^4. \tag{8}$$

Then, we obtain

$$|\psi_0|^2 \geq \frac{1}{2} + \frac{1}{2}\sqrt{2E^2 - 1} \tag{9}$$

for the ground-state population $|\psi_0|^2$. In practice, terms in Eq. (7) corresponding to higher eigenenergies will be

rather small and will destructively interfere with each other. Therefore, this bound is not tight and much smaller errors are expected in an experiment (cf. Appendix B 4).

Our protocol takes inspiration from semiclassical approaches to the quantum phase-estimation algorithm [28,29]. However, these algorithms also seek to determine the energy. As we argue above, the ground-state overlap is better suited as the cost function for algorithms for finding the ground state. Therefore, we devise the ancilla protocols, which are oblivious to the energy value at any given point.

B. Entangled-ancillas protocol

Building upon the single-ancilla protocol, we introduce a protocol using two identical quantum systems with one ancilla each. The protocol is motivated by the intuition that the single-ancilla protocol gathers information about the complex phase of $\langle\psi|\psi_{\mathrm{evo}}\rangle$, which is of no practical use to us. Instead, we would like to estimate $|\alpha|$ directly, which this protocol achieves.

We require the possibility of conducting an entangling measurement (i.e., a Bell measurement) between the two ancillas of the two systems. Such an entangling measurement could be performed with a microwave quantum link between two superconducting circuits [24]. This protocol constitutes an instance of distributed quantum computing for such a quantum network. Moreover, it is well suited to existing NISQ devices that lack an all-to-all connectivity, where the adiabatic evolutions could be implemented on separate but connected subgraphs [30].

Our goal is to determine the purity of the ancilla. In general, there is the relation that ρ is pure if and only if $\mathrm{Tr}[\rho^2] = \lambda_1^2 + \lambda_2^2 = 1$ for density matrices, where λ_1 and λ_2 are the eigenvalues of ρ. We write the density matrix and its square as

$$\rho_a = \begin{pmatrix} a & b \\ c & d \end{pmatrix} \quad \text{and} \quad \rho_a^2 = \begin{pmatrix} a^2+bc & \cdot \\ \cdot & bc+d^2 \end{pmatrix}, \tag{10}$$

where matrix elements irrelevant to our protocol are denoted with a dot. With the Bell state $|\Phi^-\rangle = (|00\rangle - |11\rangle)/\sqrt{2}$, we construct a Bell measurement. The diagonal matrix elements of ρ_a^2 may then be attained by considering a composite system where the second system has controlled negative time evolution (implementable by changing the sign of H). Then, the density matrix of the ancilla of the second system effectively corresponds to the transpose of the density matrix of the first ancilla $\rho_{a2} = \rho_{a1}^T$. The composite system gives

$$\rho_{a1} \otimes \rho_{a2} = \begin{pmatrix} a^2 & \cdot & \cdot & bc \\ \cdot & \cdot & \cdot & \cdot \\ \cdot & \cdot & \cdot & \cdot \\ bc & \cdot & \cdot & d^2 \end{pmatrix} = \frac{1}{4}\begin{pmatrix} 1 & \cdot & \cdot & |\alpha|^2 \\ \cdot & \cdot & \cdot & \cdot \\ \cdot & \cdot & \cdot & \cdot \\ |\alpha|^2 & \cdot & \cdot & 1 \end{pmatrix}. \tag{11}$$

If $|\psi\rangle$ is in an eigenstate, the density matrix of the ancilla ρ_a is pure and the expectation of the $|\Phi^-\rangle$ measurement is

$$\langle\rho_{a1} \otimes \rho_{a2}\rangle_{|\Phi^-\rangle} = \frac{1}{4}(1 - |\alpha|^2) = 0, \tag{12}$$

allowing for very-low-variance measurements when $|\psi\rangle$ is in the vicinity of the ground state. This protocol is especially well suited for hypothesis testing (cf. the Supplemental Material [26]).

V. VARIATIONAL QUANTUM ADIABATIC ALGORITHMS

Preparation of the ground state of a Hamiltonian is a problem of great significance in physics, with deep implications in the field of combinatorial optimization. While adiabatic state preparation is known to return the ground state for sufficiently long preparation times only, variational quantum algorithms require a very large number of measurements in the training phase. We present a toolbox for VQAAs. Our objective is to prepare the ground state of a problem Hamiltonian H_T with high fidelity while keeping the number of measurements in the process as low as possible. We aim at finding an optimized profile for the adiabatic evolution $H(s)$ from the ground state of H_0 to the ground state of H_T. For reasons of completeness, we refer to the Supplemental Material [26] for a treatment of the adiabatic algorithm and its implementation.

In order to find an optimized adiabatic evolution, we choose a positive resolution $L \in \mathbb{N}$ for this velocity profile and split up the adiabatic path into L chunks. Then, for every chunk $i \in \{1, \ldots, L\}$, an optimal adiabatic evolution time T_i needs to be determined (Fig. 5).

In every optimization task, it is paramount to keep the number of parameters to be optimized as low as possible.

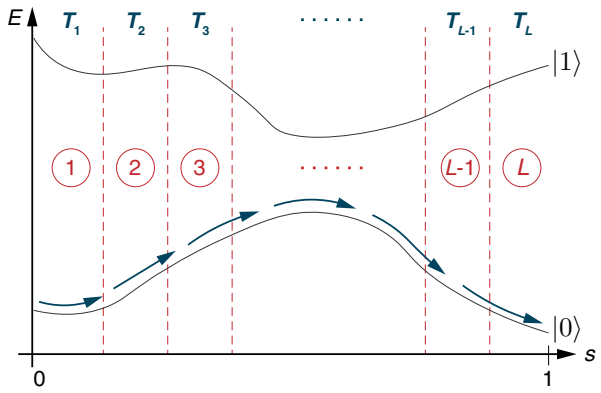

FIG. 5. An illustration of a VQAA by splitting the adiabatic path into L chunks. The ground-state and higher excited-state energies of $H(s)$ are shown here, being separated by a finite spectral gap. In an adiabatic algorithm, the ground state is prepared by following a path from a trivial Hamiltonian ground state at $s = 0$ to the target Hamiltonian at $s = 1$.

This is because every new parameter yields an additional cost in terms of the number of repetitions necessary to make all the estimations that are required in the optimization of that parameter. In a VQAA, two different options are possible. One could distribute the total time budget T for the evolution from $s = 0$ to $s = 1$ onto the L chunks (e.g., evenly spaced) and optimize the chunk lengths. Or, alternatively, one could distribute the chunks in a given way and optimize the T_i. For both options, we present suitable specific algorithms with different resource requirements. An essential ingredient for the algorithms is the ability to obtain information about the closeness of the quantum state at a given point in the adiabatic path with the ground state.

VI. PRESENTATION OF THE ALGORITHMS

The concept for the VQAA allows flexibility in the question of whether the chunk lengths or the chunk evolution times T_i are the parameters to be optimized. Also, different specific classical algorithms can be used for the optimization process. Here, we present three different algorithms for finding the chunk lengths for a fixed total evolution time and one algorithm for finding the chunk evolution times for a flexible total T. These algorithms have different resource requirements and can make use of different ground-state closeness protocols. The results stated in the abstract are obtained using the gradient-based black-box optimization for a fixed total time (Sec. VI A 3).

A. Fixed-total-time optimization

Our proposal for the VQAA allows us to set a maximum total time for the adiabatic evolution, which is well suited for the limitations of current quantum devices. Here, the total adiabatic evolution time T is allocated evenly between the chunks of the adiabatic path, so that

$$T_i = T/L \quad \forall i \in \{1, \ldots, L\}. \tag{13}$$

The chunk lengths become the variational parameters to be optimized, effectively controlling the density of the adiabatic steps.

1. Ancilla-free optimization for a fixed total time

In order to optimize $|\langle\psi(s = 1)|\mathrm{GS}\rangle|$, we try to keep the loss in fidelity in the ground-state overlap along the adiabatic path as small as possible. The chunks are initialized with equal lengths so that the end positions of each chunk are at

$$s_i = i/L \quad \forall i \in \{1, \ldots, L\}, \tag{14}$$

reproducing what we call naive QAA. The chunk lengths are $\bar{s}_i = s_i - s_{i-1}$, with $s_0 = 0$. Then, an adiabatic evolution is performed from the initial trivial product state $|\psi_0\rangle = |\psi(s = 0)\rangle = |-\rangle^{\otimes N}$ up to the end points of each chunk. This adiabatic evolution is then time reversed (at the same speed) by changing the sign in the unitaries. The total forward and backward time evolution between $s = 0$ and $s = s_i$ are described by $W_{0\to s_i}$ and $W_{0\leftarrow s_i}$, respectively, with the backward evolution being slower than the forward evolution. By going back to the initial product state $|-\rangle^{\otimes N}$, the implementation of this protocol is rather simple and allows for low-variance ground-state overlap measurements without ancillas. We denote the individual adiabatic evolution operators for chunk j from s_{j-1} to s_j in time T_j with the unitaries $V_{s_{j-1},s_j}(T_j)$, so that we write

$$W_{0\to s_i} = \prod_{j=1}^{i} V_{s_{j-1},s_j}(T_j), \quad W_{0\leftarrow s_i} = \prod_{j=i}^{1} V_{s_j,s_{j-1}}(T_j^B). \tag{15}$$

Now, we compute

$$O_i = \left|\langle\psi_0|W_{0\leftarrow s_i}W_{0\to s_i}|\psi_0\rangle\right| \tag{16}$$

for all $i \in \{1, \ldots, L\}$ with $O_0 = 1$. The consecutive ratios of the overlap are

$$R_i = \frac{O_i}{O_{i-1}} \quad \forall i \in \{i, \ldots, L\}. \tag{17}$$

These R_i correspond to the drop in ground-state overlap with each next chunk along the adiabatic path. In order to find chunk lengths that correspond to a smooth decrease of the ground-state overlaps, chunks i where the drop in ground-state overlap is larger than the average,

$$R_i > \frac{1}{L}\sum_{i=1}^{L} R_i, \tag{18}$$

are made smaller and vice versa (where R_j is below average, the jth chunk is made larger). The sum of the chunk lengths is kept normalized to one ($\sum_{i=1}^{L} \bar{s}_i = 1$). Then, new values O_i are computed and the procedure is repeated until convergence.

Clearly, what is optimized here is not exactly the instantaneous ground-state overlap because the reversed adiabatic evolution will accumulate extra phases, distorting the results slightly. Nevertheless, this method can be a useful compromise between a protocol that is very simple to execute and one that can still yield improved results for an optimized adiabatic routine (Sec. VII C 2).

2. Forward-only evolution for a fixed total time

As an improvement over the ancilla-free algorithm, this algorithm makes use of the ancilla-based ground-state

closeness protocol (Sec. IV A) in order to estimate the ground-state overlap at the point s_i in the adiabatic path

$$O_i' = \left|\langle \mathrm{GS}_{s_i}|W_{0\to s_i}|\psi_0\rangle\right|, \tag{19}$$

without backward time evolution. Here, $|\mathrm{GS}_{s_i}\rangle$ is the instantaneous ground state at point s_i of the adiabatic path. The rest of the procedure is an analog to the previous algorithm. This algorithm enables us to try to keep the quantum state along the adiabatic path close to the instantaneous ground state for a fixed total adiabatic run time.

3. Black-box optimization for a fixed total time

We present a black-box optimizer routine that makes use of the gradient to find optimized chunk lengths $\{\bar{s}_i\}$. Here, the chunk lengths are optimized in a quantum-classical feedback loop similar to typical variational quantum algorithms. In our approach, the vector containing the chunk lengths is used as the input for a quantum black box (Fig. 6). The chunk lengths remain normalized to 1. Within the quantum black box, an optimized adiabatic evolution is implemented according to the current chunk-length vector and the output of the black box is the final ground-state overlap at $s = 1$. The ground-state overlap may be obtained by, e.g., making use of our proposed one-ancilla protocol (Sec. IV A). This value of the ground-state overlap is fed into a classical optimizer, which updates the input vector. Our cost function is the ground-state overlap that we seek to maximize. We use the (quasi-Newtonian) bounded limited memory BFGS (L-BFGS-B) algorithm [31] or the gradient-free Nelder-Mead (or downhill-simplex) algorithm [32] for the classical optimization. To make the setting of the optimizer more realistic for an experimental setup, we fix the relative step size in L-BFGS-B to be larger than 1% of the chunk lengths $\{\bar{s}_i\}$. The feedback loop is repeated until convergence or until another suitable termination criterion is reached, e.g., a desired ground-state fidelity.

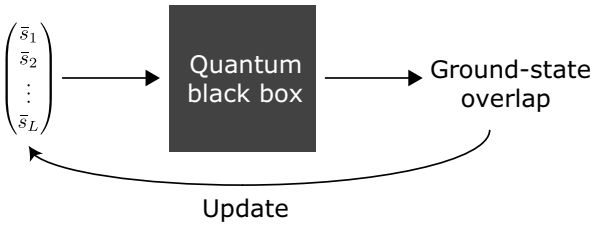

FIG. 6. The quantum-classical feedback loop for optimizing the chunk lengths of an adiabatic evolution while keeping the total time fixed. A parameter vector containing the chunk lengths is used as input for a quantum black box. The black box implements an optimized adiabatic evolution accordingly and outputs the ground-state overlap. Making use of a classical optimizer, the chunk-length vector is updated in order to maximize the ground-state overlap.

B. Target fidelity profile with a flexible total time

The concept of the VQAA also allows for flexible-total-time optimization. Here, the goal is to find an optimized adiabatic evolution that gives a final fidelity as close as possible to a given threshold

$$|\langle\psi(s=1)|\mathrm{GS}\rangle| \gtrsim \theta_L. \tag{20}$$

The adiabatic path is split up into L chunks of length s/L, with respective evolution times T_i. The state $|\mathrm{GS}\rangle$ is the ground state at the end of the adiabatic path at $s = 1$. By smoothly interpolating from θ_0 at $s = 0$ to θ_L at $s = 1$, the intermediate target thresholds θ_i are set.

Starting with the first chunk, we now search for the evolution time T_1 that suffices so that $|\langle\psi(s_1 = 1/L)|\mathrm{GS}\rangle| \gtrsim \theta_1$. Here, we can make use of hypothesis testing, which is highly efficient with regard to the number of measurements (cf. the Supplemental Material [26]). Search algorithms such as bisection methods feature exponentially fast convergence. The $\{T_i\}$ define the optimized adiabatic evolution. This algorithm is then able to follow a target fidelity profile with resolution L as closely as possible. We note that due to the limited decoherence time of NISQ devices, a maximal value for the T_i can be fixed.

VII. BENCHMARKING AND RESULTS

For benchmarking purposes, we choose a nontrivial problem where we are able to simulate the evolution of a quantum computer with and without noise on a classical computer. Simulation of the dynamics of a large quantum system on a classical computer is, in general, very hard, as the number of coefficients necessary for the classical description increases exponentially with the system size N. For this reason, we choose a gapped one-dimensional Hamiltonian as our system. In the algorithms we propose, the state is always close to the ground state, i.e., it has only a few excitations. The ground states of gapped one-dimensional systems can be described efficiently using a matrix-product-state (MPS) ansatz. We give a brief outline of the tensor-network techniques [33] that we use to simulate our algorithms classically in the Supplemental Material [26]. Therefore, even though MPS cannot approximate time evolution in general, it is ideally suited for our problem, since our states have few excitations.

A. Model

For benchmarking a simple, yet nonintegrable, quantum model, we use the translationally invariant Ising model with transverse and longitudinal fields, hereafter referred

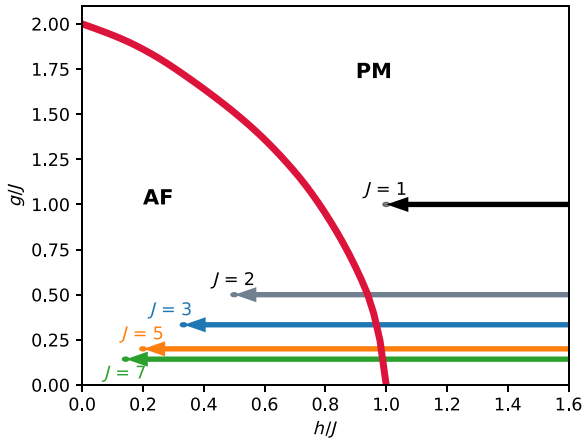

FIG. 7. The zero-temperature phase diagram of the ZZXZ model in the thermodynamic limit. The antiferromagnetic phase (AF) is separated from the paramagnetic phase (PM) by a second-order phase transition (red line). At the multicritical point at $(h, g) = (0, 2)$, the model becomes classical, resulting in a first-order phase transition. For different interaction strengths J, the adiabatic evolution follows different paths in the phase diagram. The phase diagram is after Ref. [35]: note that their different Hamiltonian formulation results in an appropriately rescaled phase diagram.

to as the ZZXZ model,

$$H_T = \sum_{i=1}^{N} (J\sigma_i^z \sigma_{i+1}^z + h\sigma_i^x + g\sigma_i^z), \tag{21}$$

as a finite system with open boundary conditions [34]. For $J > 0$, we are considering the antiferromagnetic ZZXZ model. A choice of the coefficient $J = 1$ places the model in the paramagnetic phase (Fig. 7) and an adiabatic evolution from the trivial Hamiltonian $H_0 = \sum_i h\sigma_i^x$ stays entirely within the paramagnetic phase; therefore, no phase transition is crossed [35,36]. This is different for choices—e.g., $J = \{2, 3, 5, 7\}$—where the adiabatic paths crosses a second-order phase transition from the paramagnetic phase into the antiferromagnetic phase. The adiabatic spectrum following a linear interpolation from H_0 to H_T is discrete for the lowest-energy eigenstates (for a discussion on smooth reparametrizations of the path, see the Supplemental Material [26]).

B. Results for adiabatic spectroscopy

We benchmark the adiabatic spectroscopy for the ZZXZ model on a qubit chain with $N = 53$ sites. For our model, the spectral gap $\Delta(s)$ is obtained using density-matrix-renormalization-group (DMRG) methods (Fig. 8). In our simulations, we compute the ground-state fidelity directly using tensor contractions; however, in an experiment, this information would be gathered using our ancilla protocols (Sec. IV). In an experimental setting, every time we would like to make a measurement to estimate $|\alpha(\tau)|$, we can choose to evolve uniformly at random for different values of τ between 0 and some very large K. Under these assumptions, a simple analytical formula for the expectation value E^2 of $|\alpha(\tau)|^2$ can be given (Appendix B 4) and a target ground-state fidelity of $|\psi_0|^2 = 0.8$ translates to

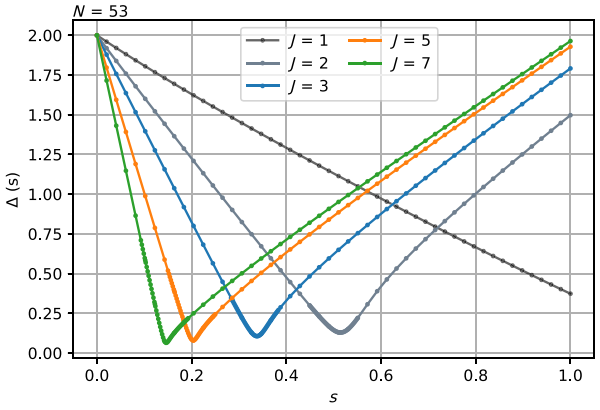

FIG. 8. The spectral gap $\Delta(s)$ for the ZZXZ model for $N = 53$ qubits and different values of J, obtained using DMRG methods. The energy difference between the ground state and the first excited state is plotted along the adiabatic path in s. The minimal spectral gap along the adiabatic path is smallest for large interaction strength J and the phase transition is crossed earlier in parametrized time s.

$$E^2 := \lim_{K\to\infty} \mathbb{E}_{\tau \sim \text{unif. dist. in } [0,K]}(|\alpha(\tau)|^2) \geq 0.68. \tag{22}$$

In the adiabatic spectroscopy, we obtain the evolution times $T(s)$ required to reach this target for a given value of s (Fig. 9). Clearly, there is a strong increase in T around the position of the minimal spectral gap for respective values of J. By computing the derivative of the (cubic) splines, we extract the position and smallness of the gap that correspond to the position and steepness of the increase in T in the $T(s)$ plot. For a closer resemblance to the actual spectral-gap profile, we plot $-\partial T(s)/\partial s$ (and clip values above zero) in Fig. 1.

C. Results for VQAA

Here, we compare the benchmarking results obtained for the different algorithms and interpret their respective behavior. In particular, we would like to highlight that there are two regimes where an optimized adiabatic path is an improvement over nonoptimized (or naive) QAA. When a phase transition is crossed in an adiabatic evolution, as intuition would suggest, optimal adiabatic paths concentrate the majority of the evolution time around the position of the spectral gap. We also examine the case without a phase transition ($J = 1$) and benchmark for systems with up to $N = 100$ qubits. Here, we observe that rotations in the low-energy eigenspace can significantly

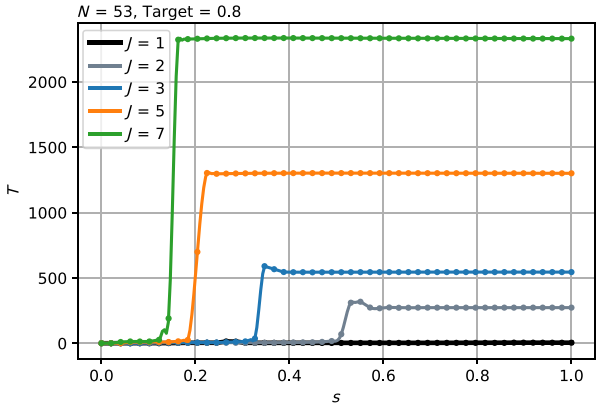

FIG. 9. Adiabatic spectroscopy for $N = 53$ qubits and a given target ground-state fidelity of 0.8. We perform adiabatic sweeps from 0 to s and find the evolution time T required to reach the target fidelity. We obtain data for 50 values of s, linearly distributed along the x axis. When a phase transition needs to be overcome, T increases to a much larger value. The steepness of the curve at this point provides a measure for the smallness of the spectral gap.

improve the performance of the quasiadiabatic evolution. Moreover, we find that leaving the instantaneous ground state can pay off in finding a better final ground-state overlap. This seems to be especially significant for short total evolution times.

1. Black-box optimization for fixed total time

The best results for a fixed time are achieved with the black-box algorithm. Even for large system sizes, this algorithm can improve significantly over naive QAA for a fixed total time. Good results are already usually achieved for a handful of chunks and the performance of the algorithm does not improve much further for a greater number of chunks (which would correspond to a higher resolution in the adiabatic velocity profile). This is the case both when a small spectral gap needs to be crossed and also in the absence a phase transition. In the latter case, the black-box algorithm very often returns an adiabatic path including one or even several very small chunks.

These rotations can be understood in the following way. The setup of the VQAA with fixed time allows some chunk length $\bar{s}_i$ to become very small. An amount of time T_i is, however, still spent in these small chunks. The evolution in such a chunk in the limit of $\bar{s}_i \to 0$ is implemented by a unitary

$$U_{\mathrm{rot}}(T_i, s_i) = e^{-iT_i H(s_i)}, \tag{23}$$

which effectively changes the local phases of $|\psi(s_i)\rangle$, thereby physically changing the quantum state. As $|\psi(s_i)\rangle$ in our algorithm is expected to have a considerable ground-state population and also small populations in the lowest excited states, the change in the local phases of $|\psi(s_i)\rangle$ corresponds to a rotation in the low-energy eigensector. Some rotations eventually become beneficial for the performance of the adiabatic routine. Rotations in the low-energy eigensector have also been considered in the context of the eigenstate thermalization hypothesis [37].

In the case of a *phase transition*, the improvement in the evolution time T between naive QAA and an optimized adiabatic evolution is much larger than without a small gap. For very few chunks only, target fidelities of over 90% in a system of 53 qubits are reached at around $T \approx 100$. With a nonoptimized adiabatic path, this would have required very long (a factor of approximately 10 longer) preparation times, as depicted in Fig. 2. The classical optimizer used for obtaining the data in this figure is the Nelder-Mead algorithm. In our simulations, Nelder-Mead proves to be more robust at large T at the expense of requiring more measurements. Being a gradient-free method, we expect it to behave better than the gradient-based L-BFGS-B for noisy systems.

In Fig. 10, the evolution of the chunk positions for an instance of the black-box algorithm is shown for 53 qubits and $J = 3$. Here, the total time is $T = 5$ and L-BFGS-B is chosen as the classical optimizer due to its faster convergence in the classical simulations. The adiabatic spectrum for $J = 3$ features a small gap around $s = 0.34$. This can be captured approximately with only three chunks. Over a few iterations, the center chunk becomes smaller around the position of the gap, so that in the adiabatic evolution more time is spent there.

In the case *without a phase transition*, for $J = 1$, we find reductions of the total evolution time by a factor of over 3 when comparing with naive QAA. Here, we benchmark

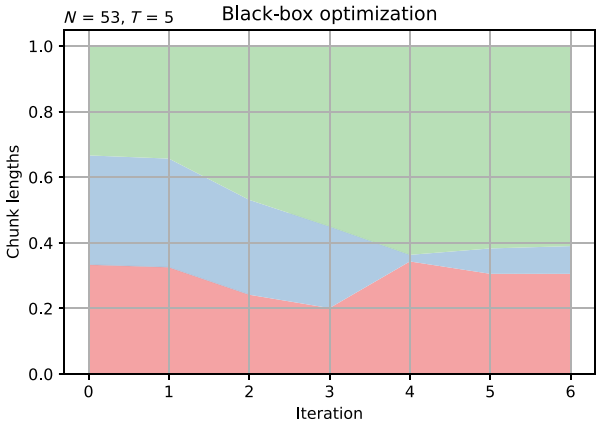

FIG. 10. An instance of a black-box optimizer for the case when crossing a phase transition, here for $J = 3$ and $N = 53$. The stacked chunk lengths are shown for the first nine iterations as the middle chunk becomes smaller. This leads to the evolution time being spent effectively around the smallest gap around $s \approx 0.34$. In this instance, the final fidelity is nearly 7 times larger using the VQAA compared with a linear sweep.

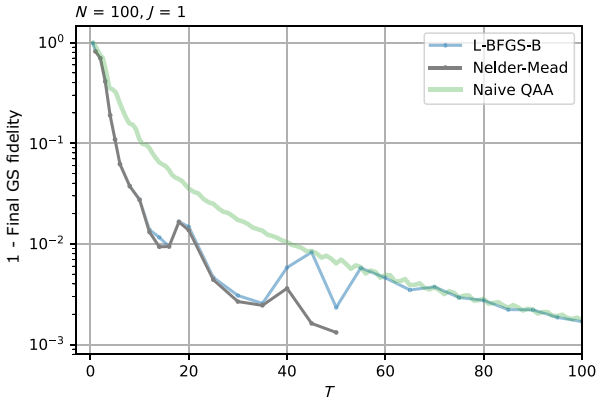

FIG. 11. The large-T black-box optimizer benchmark for the two classical optimization algorithms L-BFGS-B and Nelder-Mead (NM). The data for NM are only obtained up to $T = 50$ and require, in general, more measurements than gradient-based methods. However, the optimization with L-BFGS-B becomes increasingly unstable for large $T > 40$ and NM is observed to be more robust, because a very large amount of fine tuning of the initial step size is required for the different values of T.

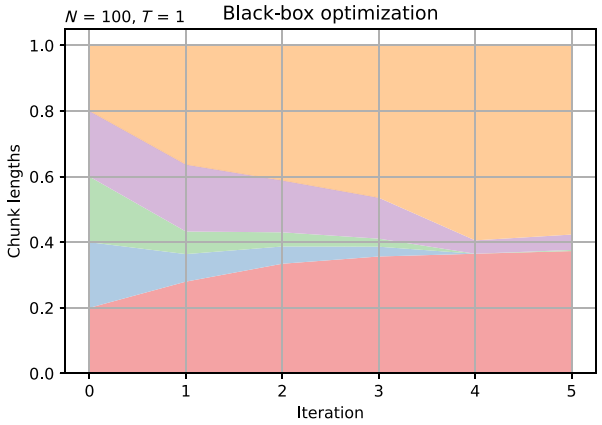

FIG. 12. Stacked chunk lengths adding to $s = 1$ display the evolution of an instance of a black-box optimizing routine. The chunks are initialized with equal lengths and their lengths are optimized using a L-BFGS-B optimizer with regard to a maximal final fidelity with the ground state of the ZZXZ Hamiltonian. A confluence of chunks can be observed around $s \approx 0.4$.

the black-box optimization routine for large values of T and 100 qubits (Fig. 11). We note that for $T > 40$, the classical L-BFGS-B algorithm is in most cases unable to find an optimized adiabatic path. We make sure that this is not due to memory limitations in the optimizer, the relative step size, or tolerance values for the termination of the algorithm. Increasing the number of chunks does not generally help in finding better-optimized paths. However, sequential initializations of the optimizers can improve the performance. Instead of starting with naive QAA, the optimizer then begins with the chunk lengths of the previous shorter-time optimizer instance.

A typical black-box algorithm instance (for $J = 1$, i.e., no small gap) is shown in Fig. 12, where the small chunks can be easily observed around $s \approx 0.4$. Indeed, the ground-state fidelity is maximized and the energy minimized in only five iterations. In Fig. 13, the fidelity between $|\psi(s)\rangle$ and the ZZXZ ground state or the instantaneous ground state of $H(s)$, respectively, is shown. The exact ground states are obtained using DMRG methods. A discontinuity in the path of the optimized QAA is clearly visible for $s \approx 0.4$ due to the implemented rotation. As the black-box optimizer only has access to the ground-state overlap at $s = 1$, it is agnostic to the actual curve of the optimized QAA for values below $s < 1$. It is interesting to observe that, in fact, leaving the instantaneous ground state can lead to better final results at $s = 1$, as also discussed for adiabatic evolutions in Ref. [38] and in a related way, in the context of diabatic transitions in QAOA, in Ref. [39]. This feature can also be observed in a black-box optimizer instance for a smaller system in Fig. 14, where the optimized QAA curve gives a final fidelity of approximately 0.999 and recovers most of its ground-state fidelity in only the last 20% of the adiabatic evolution path.

2. Converging fidelity ratios for a fixed total time

Besides the black-box approach to VQAA, we present other algorithms that aim to stay close to the instantaneous ground state along the adiabatic path. Both the ancilla-free and the one-ancilla method seek convergence in the fidelity ratios between consecutive chunks. The one-ancilla method is cleaner in the sense that it directly uses the overlap and does not accumulate extra transitions and phases on the backward path (Sec. VI A 2). The one-ancilla method can achieve a smooth adiabatic path that remains as close as possible to the ground state at all times for a fixed total evolution time. However, the ancilla-free method finds adiabatic paths that effectively implement a rotation in the low-energy eigensector. This property is also observed in the gradient-based black-box method (Sec. VII C 1) and seems to be very relevant for preparation of the ground state on NISQ devices. Therefore, for these two algorithms, which method will perform better is likely quite model dependent.

3. Target fidelity profile for a flexible total time

The flexible-total-time algorithm with a given target fidelity with the ground state at the end of the adiabatic evolution is well suited in the kind of instances in which staying close to the ground state is desired. As we observe in Fig. 15, the naive QAA will occasionally leave the ground state, leading to oscillations in the instantaneous ground-state fidelity. Considering the adiabatic path split up into several chunks, due to the changing Hamiltonian $H(s)$, different evolution times $\{T_i\}$ for each chunk are

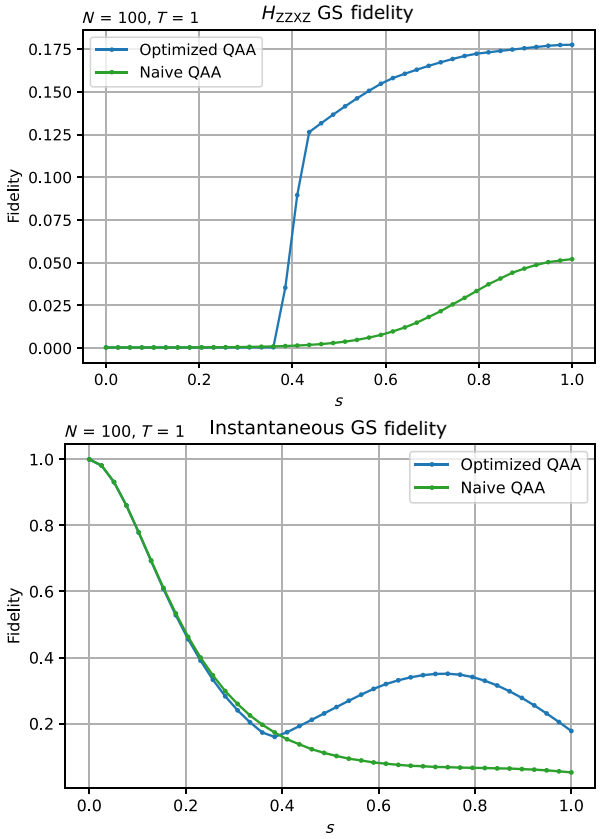

FIG. 13. The ground-state fidelity is plotted along the adiabatic path for different values of s. The results are for $N = 100$ and fixed total time $T = 1$. The optimized QAA curve (blue) differs significantly from naive QAA (green curve) in the region of very small chunks around $s \approx 0.4$. Note that the spectral gap between the ground state and the first excited state is not minimal in this region but decreases strictly monotonically with s. At the end of the evolution, optimized QAA achieves a ZZXZ model ground-state fidelity of 17.8%, while naive QAA results in a fidelity of 5.2%.

necessary in order to achieve a given fidelity with the ground state at the end of the adiabatic evolution. The values for the $\{T_i\}$ depend strongly on the spectral gap $\Delta(s)$ between the ground state and the excited state, as well as on the Berry connections (cf. the Supplemental Material [26]).

We observe that our algorithm is able to reduce the total adiabatic evolution time compared to naive QAA in this toy example. This is because it uses the time available in a more economic way by spending much of the evolution time only when required to stay close to the ground state. One useful property of this algorithm is the fact that it is self-verifying in the sense that the hypothesis testing at the end of every chunk guarantees, with high confidence, that the ground-state fidelity is larger than a given value. Further developments of this algorithm can be envisioned where the $\{T_i\}$ are optimized to follow a more

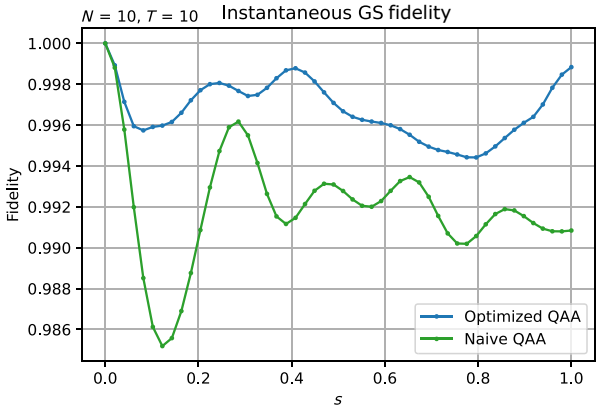

FIG. 14. In this instance, albeit for $N = 10$, we see near perfect ground-state preparation for $T = 10$ without increasing the total time budget. Even though the instantaneous ground-state fidelity with $H(s)$ along the adiabatic path is smaller, the final ground-state fidelity is 0.999.

complicated profile. Moreover, the results of this algorithm serve as a good initial point for the gradient-based black-box algorithm for a fixed total evolution time.

Here, we set the chunk lengths $\{\bar{s}_i\}$ to equal values. Adaptations of this algorithm with unevenly spaced chunks are also possible. The inclusion of additional chunks with a very small chunk length could possibly provide better performance of the algorithm by making it possible to implement rotations in the low-energy eigensector at the expense of an increased number of measurements (Sec. VII C 2).

D. Implementation cost

In every variational algorithm, the number of measurements needed in order to obtain satisfactory results is of

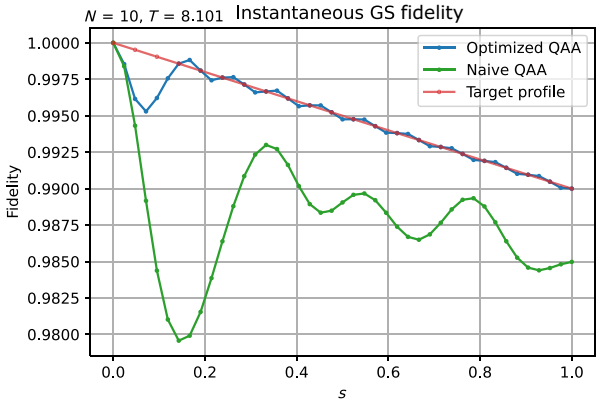

FIG. 15. The instantaneous ground-state fidelity for QAA optimized with the flexible-total-time algorithm compared to naive QAA with the same time budget. The target fidelity at $s = 1$ is set to $\theta = 0.99$ and linearly interpolated along the adiabatic path. The search interval for the time spent in each chunk is upper bounded such that $T_i \leq 20\ \forall i$.

the utmost importance, as it directly determines the feasibility of the approach. Here, we discuss the number of measurements necessary for each of the respective algorithms presented in this paper. We focus on the number of ground-state overlap evaluations necessary in our classical simulations. To obtain the ground-state overlap from $|\alpha|$, a small overhead is required (Sec. IV A).

Both the *ancilla-free and the one-ancilla fixed-time algorithms* converge with very few iterations even for large system sizes ($N = 100$). The resolution of the velocity profile in the adiabatic evolution is the number of chunks chosen. In our case, the number of ground-state overlap evaluations is fairly low, with

$$\begin{aligned}&\text{number of GS overlaps}\\&\quad = \text{number of iterations} \times \text{number of chunks} \lesssim 100,\end{aligned} \tag{24}$$

which suffices for our simulations. The number of chunks is the number of parameters to be estimated and for the *flexible-total-time algorithm* this corresponds to the number of bisection searches required. As these search algorithms converge exponentially fast, roughly 10–20 ground-state overlap estimations per search are usually sufficient for the highest accuracies of the optimized $\{T_i\}$ values. In this algorithm, the two-ancilla algorithm is used, which is suitable for hypothesis testing. The hypothesis testing converges exponentially fast as well, requiring about another ten measurements for each ground-state overlap estimation. Exemplary numbers for hypothesis testing are given in the Supplemental Material [26].

The *black-box algorithm* depends on ground-state overlap evaluations in order to estimate the gradient. The number of ground-state overlap evaluations necessary in the optimization process is directly related to the number of chunks. Good results can already be obtained using this method with just a few iterations, so that for five chunks, we achieve good results for $N = 100$ and $T = 1$, with significantly fewer than 50 ground-state overlap evaluations in total (Fig. 19). For a random variable X with values in $[a, b]$, $\bar{\Delta} = b - a$ and independent and identically distributed samples, the Chernoff-Hoeffding inequality [40] gives an upper bound on the probability of finding the measurement deviating more than ϵ from its expectation value μ:

$$\Pr(|X - \mu| \geq \epsilon) \leq e^{-2m\epsilon^2/\bar{\Delta}^2} =: \eta. \tag{25}$$

For Pauli measurements, we can have either $+1$ or -1 as results, so $\bar{\Delta} = 2$ and the number of measurements

$$m \geq \frac{2}{\epsilon^2} \log\left(\frac{1}{\eta}\right) \tag{26}$$

depends on the η and ϵ needed. Setting the precision ϵ to $[1 - (\text{GS fidelity})]/20$ and the failure probability so that one in two experiments is successful with all estimations within the deviation ϵ, we estimate the number of measurements necessary to be of the order of 10^3.

The number of ground-state fidelities required to reach very high fidelities > 0.9 at larger T is naturally larger than what is stated above for $T = 1$. In Fig. 2, the maximum number of ground-state fidelity evaluations is set to 1000, while typically a few hundred evaluations suffice to find an adiabatic path with a maximal ground-state fidelity up to 10^{-8} relative accuracy (i.e., the relative accuracy of the optimization process). Without doubt, this accuracy is unattainable in current experiments and many fewer ground-state evaluations already give very good results. In fact, we observe that for $N = 53$ in the case of a phase transition and $T \approx 100$, when obtaining fewer than 200 ground-state evaluations, the Nelder-Mead method yields results of practically the same quality. These estimations suggest a very low number of measurements even for optimizing the adiabatic evolution of large quantum systems.

While the number of measurements seems to be the most relevant figure of merit to assess the cost of the methods presented here, we also include a short discussion of the number of gates required on different architectures of quantum devices. On analog quantum simulators, for instance, the ancilla-free optimization method can be implemented natively, with the only overhead being the additional parametrized adiabatic sweeps to find optimized adiabatic paths. In a gate-model architecture, for a qubit-chain with $N = 53$ sites and only allowing for nearest-neighbor interaction, we upper bound the total number of controlled-NOT (CNOT) gates for one unit of time at around 120 CNOTs per N. Here, we consider a decomposition of the unitary gates in the Trotterized evolution of the numerical simulation. The actual number of gate counts is significantly lower, because the circuit is optimized for the respective experimental hardware platform. In the single-ancilla protocol, an upper bound on the number of CNOTs per unit of time ($\tau = 1$) including the required SWAP gates for the chain topology is set at around 2100 CNOTs per N. We note that with τ scaling as the inverse of the spectral gap $\Delta(s)$, the cost of the protocol is not excessively demanding, especially at the end of the adiabatic sweep ($s = 1$) where the gap is large. A more detailed discussion of the gate count is provided in the Supplemental Material [26].

VIII. NOISE

A. Noise in adiabatic quantum computation

The noise in current quantum devices severely limits the performance of many quantum algorithms [41]. Therefore, we discuss some important properties of noisy quantum adiabatic algorithms. A general inherent robustness of adiabatic evolution has already been established for some

time [42]; here, we focus on a few points that are especially important to our method.

In a gate-model quantum algorithm without error correction, a flipped qubit will in the worst case render the whole quantum computation nonsensical. This is quite different in an adiabatic algorithm, as for physical instances, low-energy spectral lines are rare [Fig. 21(a)]. While a flipped qubit in the preparation of the ground state in an adiabatic algorithm can also lead to a quantum state orthogonal to the ground state, the energy, however, of this orthogonal excited state will still be a very good approximation to the ground-state energy. Intuitively, one bit flip corresponds to a single excitation of the system. We can therefore assume that errors increase the energy only by $\mathcal{O}(1)$ for fixed time, when flipped qubits are rare. Also, the position s_0 in the adiabatic path, where a flipped qubit occurs, is not critical [Fig. 21(b)]. This may seem somehow surprising but it can be explained because a perfect adiabatic evolution suppresses all transitions between the eigenstates. It does not only apply to the ground state but also to excited states. Therefore, in the regime of an adiabatic evolution, a noise-induced excitation will not lead to further deviations from the ground-state energy.

However, for time evolutions that are faster than an adiabatic evolution, which is in general the case for quantum devices limited in coherence time, we would generally expect light-cone spreading of noise through the spin chain. Yet, in our simulations this is not observed to be problematic for the performance of the VQAA. In general, the noise behavior of adiabatic algorithms is encouraging, as it suggests very benign noise features in these kinds of algorithms, making them a suitable candidate for NISQ devices.

B. Impact of noise in the presented algorithms

Here, we include a qualitative discussion about the expected performance of the algorithms presented in this paper in the presence of noise. We expect the *adiabatic spectroscopy* to be quite robust to noise, as the information obtained using this method relies on multiple data points and a rather distinctive feature in the $T(s)$ curve resulting from a small spectral gap. Noise effects will become stronger toward the end of the adiabatic evolution as noise accumulates in the circuit. However, as the results of this spectroscopy are quite pronounced, a qualitative description of the gap is likely only slightly impaired by moderate noise in the circuit.

Regarding the *VQAA algorithms*, when considering noise, there are two main points to consider. First, noise can substantially impede the training phase of the algorithm, when the search is for the parameters of an optimal adiabatic path. Second, in order to prepare the ground state with a desired high fidelity, an adiabatic evolution time T that is only a fraction of the T required for naive QAA suffices with an optimal adiabatic path. This may help strongly in suppressing errors.

Following a *target profile* is especially tricky when noise comes into play. This is because noise strongly alters the required target profile. Therefore, concerning the target profile method, we do not expect this method to be very robust to noise, especially when finite-size effects are playing a role. In the presence of noise, optimizing with regard to the final ground-state overlap instead is thus advisable.

For the *black-box method*, in classical simulations with noise, we observe that the gradient-based training is not too well behaved. Convergence to optimized paths that improve over naive QAA is often impossible even when only a few bit flips occur in the quantum circuit. Classical optimization routines that are more robust toward noise seem to be required here, i.e., a classical optimizer that is combined with an error-mitigation technique so that noisy outputs of the quantum black box can be corrected. We note that gradient-free optimization methods are expected to be more robust to noisy environments and could provide better performance in an experimental setup than a gradient-based method. For this reason, we make use of the COBYLA method [43]. In Fig. 16, it can be observed that small amounts of noise significantly impair the training process of an optimized adiabatic path. For small noise strengths p, however, the results can be an improvement even over naive QAA. For simulating the noisy quantum circuit, 100 MPS samples are taken. For more details on the noise model, we refer to the Supplemental Material [26].

Besides noise in the adiabatic evolution, noise also is present in the measurement process. For both the

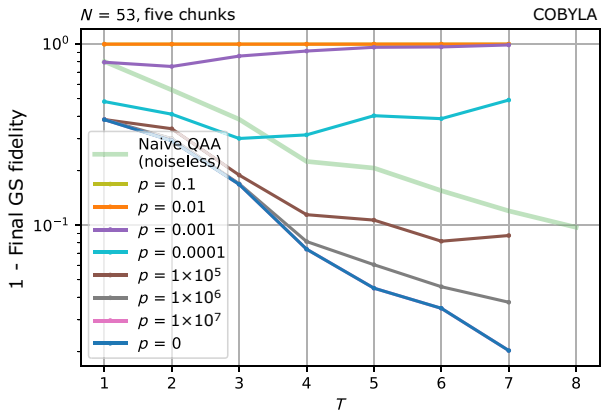

FIG. 16. The noisy benchmark of the black-box algorithm for $N = 53$, $J = 1$, and a maximum of seven optimizer iterations. The noise strength p determines the expected number of noisy qubits. Noise is applied in the circuit both in training and in the testing phase. The pink curve ($p = 10^{-7}$) lies behind the blue curve due to the very rare noise events (cf. the Supplemental Material [26]). No measurement noise is considered and naive QAA is given as a reference without noise. COBYLA is used as the classical optimizer.

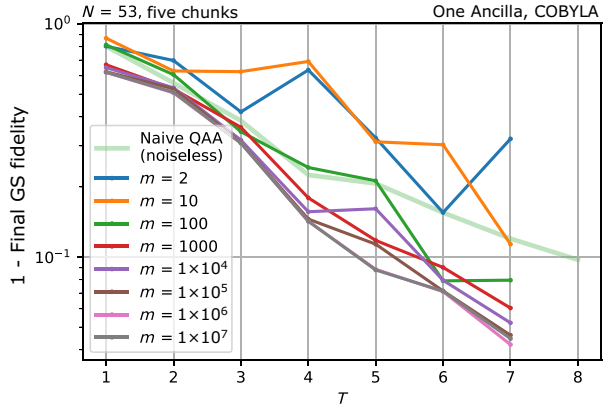

FIG. 17. The simulation of shot noise in the black-box algorithm for $N = 53$ and $J = 1$ using the one-ancilla method. The number of measurements taken for every ground-state overlap estimation is given by m. Note that no extra noise is applied during the circuit. COBYLA is used as the classical optimizer. For $m > 10^3$, the results begin to converge and the shot noise is sufficiently small.

one-ancilla method and the two-ancilla method, we benchmark the black-box routine numerically. The shot-noise simulation is performed by finite sampling of m independent measurements and taking the average of these measurements. From the numerical data, we can conclude that for a large system, around 10 000 measurements can reduce the shot noise sufficiently. This is one order of magnitude larger than the estimations made earlier, in Sec. VII D. The benchmark for the one-ancilla method is shown in Fig. 17, while the plot for the two ancilla method can be found in Fig. 22 (Appendix C).

A further comment is needed to specifically address the noise in the black-box algorithm, which makes use of a gradient to optimize the adiabatic path. In a recent work, it has been shown that the gradient in a variational quantum algorithm vanishes exponentially with the number of qubits N when the number of layers scales as poly(N) [18]. These noise-induced barren plateaus severely hinder the scalability of variational quantum algorithms on NISQ devices. In our work, however, the algorithms either optimize the adiabatic path for a fixed total evolution time (which includes the gradient-based black-box algorithm) or have a maximum time budget in the case of the target-fidelity-profile algorithm. Thus, the (maximum) circuit depth is fixed in our approach, which makes the results on noise-induced barren plateaus not directly applicable.

IX. DISCUSSION

In this paper, we present a toolkit for quantum adiabatic computation. This toolkit includes a proposal for adiabatic spectroscopy and ancilla protocols for estimating the ground-state overlap, as well as the VQAA as a flexible yet powerful framework for variationally optimized adiabatic paths for high-fidelity ground-state preparation.

The *adiabatic spectroscopy* offers a straightforward approach to obtaining information about an adiabatic spectrum. Our method relies on protocols to evaluate the closeness of an N-qubit quantum state $|\psi\rangle$ to an eigenstate using controlled unitary evolution. By remaining sufficiently adiabatic throughout the evolution, a self-consistent argument applies, enabling us to identify this eigenstate with the ground state. We note that the error in the ancilla protocols presented is smallest when being close to an eigenstate. The protocol that we propose requires the ability to implement controlled time evolution on a single-ancilla qubit. Current technology already meets the requisites of our protocol: conditional dynamics have been explored in the context of trapped-ion simulators and Rydberg-atom arrays [44,45] and they can be implemented efficiently in a gate model.

A natural requirement for the spectroscopy is that the decoherence time of the quantum device is not a limiting factor to determining the evolution time required in order to reach the target overlap. The applications of the adiabatic spectroscopy go beyond obtaining the spectral gap for a given Hamiltonian $H(s)$. By aggregating spectral information from several adiabatic paths that cut through the phase diagram of a target Hamiltonian H_T, rich properties of quantum many-body systems may be acquired.

We note that the numerical results presented in Fig. 1 support our argument that this technique is suitable for the derivation of information about the spectral gap. However, the relation $\partial T(s)/\partial s \sim 1/\Delta(s)^2$, which is obtained from the LZ model, is only a first-order approximation. Improvements of the quantitative validity of the adiabatic spectroscopy are left for future work and might build upon the rich literature on adiabatic perturbation theory [46].

We now discuss the *VQAA* from two perspectives: first, the perspective of VQAA as a quantum algorithm for optimal adiabatic paths; and, second, the VQAA as a variational quantum algorithm that requires only a few measurements.

Adiabatic quantum computation is known to prepare the ground state of a target Hamiltonian H_T for a sufficiently long preparation time T. However, T scales as a function of the minimal spectral energy gap $\Delta(s)$. For general H_T, the best rigorous bound on T has a inverse cubic gap dependence $T = \mathcal{O}\{[\min_s \Delta(s)]^{-3}\}$ [11]. Due to the limited decoherence time of NISQ devices, the large evolution times necessary for high-fidelity ground-state preparation can be a difficulty. If it was possible to reduce T to fit into the coherent time frame of a quantum device, it would become possible to adiabatically prepare ground states, e.g., the solution of an optimization problem, which has remained unattainable up to now.

The question of finding an optimal path for the adiabatic evolution has already been the focus of research efforts for several years and for the unstructured search problem, the Grover-type speed-up has been recovered using an optimized adiabatic sweep [15]. However, the position and size of the spectral gap are, in general, *a priori* unknown and it can be as hard a problem to obtain the spectral properties of the adiabatic path as it can be to prepare the ground state. Therefore, the question of how an optimized adiabatic path can be obtained when no or only little spectral information is available remains a challenge. One recent work has employed techniques from reinforcement learning to find an optimal adiabatic path [47]. In our work, we phrase the problem of finding an optimized adiabatic path as a problem to be solved through a variational quantum algorithm with a step-wise adiabatic velocity profile.

Turning now toward a discussion of the VQAA as a variational algorithm, we begin by noting that the ground-state overlap can be a suitable cost function for quantum-classical feedback loops. Variational approaches such as the quantum approximate-optimization algorithm (QAOA) [17] have sparked intensive research interest in recent years. The number of measurements necessary to estimate an objective function scales with $\mathcal{O}(\epsilon^{-2})$, where ϵ is the maximum error that can be tolerated in the optimization process. The proposal of the VQAA aims to reduce the number of measurements by requiring relatively fewer parameters that need to be optimized and by considering a cost function with a low variance.

Variational approaches for preparing a ground state generally make use of the energy as a cost function and that energy is estimated via the local observables that compose the Hamiltonian [48]. As the actual ground state will generally not be an eigenstate of the Hamiltonian local terms (e.g., if there is frustration), a low variance in the estimates cannot be guaranteed. Moreover, the orthogonal eigenstates in the low-energy sector typically yield similar energy values, hindering convergence to the ground state. If we were indeed able to directly measure in the eigenbasis of the Hamiltonian at a given point in the adiabatic path, we would seek to exploit the property of proximity to an eigenstate, which is inherent to adiabatic algorithms. The textbook approach for this problem would be a quantum phase-estimation (QPE) algorithm and direct implementation requires an ancilla overhead [22]. Recent semiclassical approaches are able to use a single ancilla only by utilizing postprocessing schemes [28,29]. For the VQAA, we suggest the overlap with the ground state as a figure of merit. In the case of the adiabatic algorithm, the optimal value of some other figures of merit, such as the energy, are not directly accessible. Therefore, we present two protocols to evaluate the closeness to an eigenstate using controlled unitary evolution. The entangled-ancillas protocol offers the possibility of performing low-variance measurements by harnessing the power of hypothesis testing when being close to an eigenstate. We note that in the case of a small spectral gap, e.g., when a phase transition is crossed, the ground-state overlaps are in general very small and special care is needed to extract useful information with the ancilla protocol.

In the limit of very large depth, the QAOA has the possibility of recovering a Trotterized adiabatic evolution. Therefore, a black-box VQAA algorithm bears some similarities to the QAOA. Several key differences are remarked upon, though. First, analogous to the evolution times in a (Trotterized) adiabatic evolution, the unitaries in the QAOA feature *angles* as parameters. However, for a quantum cost function H_T, the optimized angles could be too large for the decoherence limit of the NISQ device on which the algorithm is supposed to be implemented. On the contrary, limiting the maximum angles could be rather problematic for the performance of the QAOA. This issue does not arise in the black-box VQAA, as the total evolution time is fixed. Second, even for large system sizes with 53 or 100 qubits, the VQAA is a significant improvement over naive QAA for a very small number of parameters L only. In the QAOA, it is generally expected that deep circuits are necessary to obtain good results for large systems. Finally, even for very small L, the performance of the VQAA is lower bounded by the QAA with a linear time profile. This is true for the QAOA only when the angles are initialized akin to a Trotterized adiabatic evolution, which requires a large-depth QAOA.

X. SUMMARY AND OUTLOOK

We seek to combine the best from two worlds by combining the strengths of the adiabatic and the variational approaches. We present a toolbox for the VQAA building upon ancilla-based methods to evaluate the ground-state fidelity at any point in the adiabatic path. Our approach only obtains information about the proximity to the ground state and is deliberately oblivious to the actual value of the energy throughout the adiabatic path. Due to the small parameter space and the ground-state overlap as our cost function, the number of measurements necessary in the optimization of the adiabatic evolution is dramatically lower than for typical variational quantum algorithms such as the QAOA. On the whole, our work suggests that a further exploration of NISQ algorithms based on variational adiabatic concepts is indicated.

For instance, there seems to be room for sequential VQAA algorithms. In some instances, when going toward larger T, the black-box VQAA does not improve in a strictly monotonous manner. By reusing information from shorter T, the optimized paths for larger T might be improved upon and obtained more rapidly. In a similar direction, it will be interesting to see how the information gathered through adiabatic spectroscopy is used for the optimal adiabatic path in an experimental setting. If

it was possible to use adiabatic spectroscopy to eliminate or drastically reduce the quantum-classical training phase of the VQAA, this would surely be a large advancement in NISQ algorithms for ground-state preparation. Also, it remains to be seen what bounds can be established on how quickly and closely the VQAA can find an adiabatic path that is optimal.

Furthermore, there is increasing research interest in error-mitigation techniques for NISQ devices [49,50] and a further exploration of how the VQAA might benefit from these techniques appears promising. More generally, the protocols for estimating the ground-state overlap presented in this work could make a wide range of new exciting quantum algorithms for ground-state preparation possible. This might include the opportunity for an algorithm to find optimized adiabatic paths using techniques from reinforcement learning or a combination of the protocols with techniques such as projected measurements and the quantum Zeno effect [51]. Besides, in the regime where the time evolution is not strictly adiabatic, high final ground-state fidelities might be achieved by not starting in the ground state of the initial Hamiltonian but in an appropriate superposition in the low-energy sector of the initial Hamiltonian.

ACKNOWLEDGMENTS

We thank M.C. Bañuls, T. O'Brien, S. Lu, D. Wild, A. Sauer, and F. Pollmann for insightful discussions. We acknowledge support from the European Research Council (ERC) Advanced Grant "Quantum Emitters in Non-Conventional Baths" (QUENOCOBA) under the European Union Horizon 2020 program (Grant Agreement No. 742102) and the ERC Starting Grant FINE-TEA-SQUAD under the Horizon Europe program (grant agreement 101040729) and from the Deutsche Forschungsgemeinschaft (DFG, German Research Foundation) under Project No. 414325145 in the framework of the Austrian Science Fund (FWF): SFB F7104. B.S. was supported by the German Academic Scholarship Foundation (Studienstiftung des deutschen Volkes).

Note added.—After the completion and submission of this paper, some of the variational adiabatic methods presented here have been tested experimentally using large arrays of neutral Rydberg atoms to prepare the ground state of the maximum-independent-set problem on unit disk graphs with disorder [52].

APPENDIX A: ADIABATIC STATE PREPARATION IN THE LANDAU-ZENER MODEL

We seek to better understand adiabatic spectroscopy as presented in the main text. Therefore, we would like to obtain a qualitative relation between the spectral gap $\Delta(s)$ along the adiabatic path and the evolution time $T(s^*)$ required to prepare the ground state of $H(s^*)$ with a given target fidelity. In order to do so, we turn toward the well-known LZ model, which describes a simple two-level system [53,54]. The model Hamiltonian is given as

$$H = \lambda(t)\sigma^z + g\sigma^x = \begin{pmatrix} \lambda(t) & g \\ g & -\lambda(t) \end{pmatrix}. \tag{A1}$$

With $\tan\theta = g/\lambda(t)$, we write the eigenvectors as

$$|a\rangle = \begin{pmatrix} \sin(\theta/2) \\ -\cos(\theta/2) \end{pmatrix} \quad \text{and} \quad |b\rangle = \begin{pmatrix} \cos(\theta/2) \\ \sin(\theta/2) \end{pmatrix}. \tag{A2}$$

The eigenenergies are given as $E_\pm = \pm\sqrt{\lambda(t)^2 + g^2}$ and the coupling is assumed to be a linear function in time $\lambda(t) = \delta t$. This implies that the minimum of the spectral gap (the avoided level crossing) is found at $t = 0$, i.e., an adiabatic evolution parametrized by s from 0 to the position of a small gap s^* is understood to be mapped onto the LZ evolution from very small initial t to $t = 0$.

A perturbative approach yields the probability

$$|\alpha_+(t_f)|^2 \approx \frac{\delta^2}{16g^4}\left\{\frac{g^6}{[g^2+\lambda(t_i)^2]^3} + \frac{g^6}{[g^2+\lambda(t_f)^2]^3}\right\} \tag{A3}$$

of finding the system in the excited state at t_f after initializing in the ground state at t_i [55]. Assuming the beginning of the adiabatic evolution at $t_i = -\infty$, we are given

$$|\alpha_+(t_f)|^2 \approx \frac{\delta^2}{16g^4}\frac{g^6}{[g^2+\lambda(t)^2]^3} = \frac{\delta^2 g^2}{16E_+(t)^6} \tag{A4}$$

where we identify t with t_f. Now, we set a target fidelity $A_+^2 := |\alpha_+(t)|^2$ and assume that the total evolution time T scales as $T \sim 1/\delta$:

$$T \sim \frac{1}{\delta} \approx \frac{g}{4A_+E_+(t)^3}. \tag{A5}$$

As we are interested in the change of T, we compute the time derivative of T,

$$\dot{T} \sim -\frac{3}{4}\frac{g\delta}{A_+E_+(t)^5} = -3\frac{1}{E_+(t)^2}, \tag{A6}$$

where we use Eq. (A5) in Eq. (A6). Because of $\Delta(t) = 2E_+(t)$ in the LZ model, we obtain $\dot{T} \sim 1/\Delta(t)^2$ as an approximation to the scaling of $\dot{T}$ up to coefficients and possible corrections.

APPENDIX B: CALCULATIONS FOR THE ONE-ANCILLA AND ENTANGLED-ANCILLAS PROTOCOL

1. Single-ancilla protocol

The combined system after the unitary evolution can be written as

$$\text{C-}U\,|\psi\rangle\,|+\rangle = \frac{1}{\sqrt{2}}\left[|\psi\rangle\,|0\rangle + U\,|\psi\rangle\,|1\rangle\right] =: |\zeta\rangle\,. \quad \text{(B1)}$$

Denoting the quantum state after the unitary evolution as $|\psi_{\text{evo}}\rangle = U|\psi\rangle$, we note the following relationships regarding Pauli measurements of the ancilla:

$$\langle\zeta|\mathbb{1}\otimes\sigma_x|\zeta\rangle \quad \text{(B2)}$$

$$= \frac{1}{2}\left[\langle 0|\,\langle\psi|\,U\,|\psi\rangle\,|0\rangle + \langle 1|\,\langle\psi|\,U^\dagger\,|\psi\rangle\,|1\rangle\right] \quad \text{(B3)}$$

$$= \frac{1}{2}\left[\langle\psi|\psi_{\text{evo}}\rangle + \langle\psi_{\text{evo}}|\psi\rangle\right] = \text{Re}(\langle\psi|\psi_{\text{evo}}\rangle) \quad \text{(B4)}$$

and

$$\langle\zeta|\mathbb{1}\otimes\sigma_y|\zeta\rangle \quad \text{(B5)}$$

$$= \frac{i}{2}\left[\langle 0|\,\langle\psi|\,U\,|\psi\rangle\,|0\rangle - \langle 1|\,\langle\psi|\,U^\dagger\,|\psi\rangle\,|1\rangle\right] \quad \text{(B6)}$$

$$= \frac{i}{2}\left[\langle\psi|\psi_{\text{evo}}\rangle - \langle\psi_{\text{evo}}|\psi\rangle\right] = -\text{Im}(\langle\psi|\psi_{\text{evo}}\rangle), \quad \text{(B7)}$$

so that

$$\langle\psi|\psi_{\text{evo}}\rangle = \langle\sigma_x - i\sigma_y\rangle_{\text{ancilla}} = \left\langle\begin{pmatrix}0 & 0\\ 2 & 0\end{pmatrix}\right\rangle_{\text{ancilla}}. \quad \text{(B8)}$$

For a fixed Hamiltonian $H = \sum_j E_j\,|\phi_j\rangle\,\langle\phi_j|$ with the unitary $U|\phi_j\rangle = e^{-iH\tau}\,|\phi_j\rangle = e^{-iE_j\tau}\,|\phi_j\rangle$, we write the state $|\psi\rangle = \sum_j \psi_j\,|\phi_j\rangle$ in the eigenbasis of H with $|\psi\rangle$ normalized ($\sum_j |\psi_j|^2 = 1$). The total quantum system can be expressed as

$$|\zeta\rangle = \frac{1}{\sqrt{2}}\left[|\psi\rangle\,|0\rangle + U\,|\psi\rangle\,|1\rangle\right] \quad \text{(B9)}$$

$$= \frac{1}{\sqrt{2}}\left[\left(\sum_j \psi_j\,|\phi_j\rangle\right)|0\rangle + \left(\sum_j e^{-iE_j\tau}\psi_j\,|\phi_j\rangle\right)|1\rangle\right] \quad \text{(B10)}$$

$$= \frac{1}{\sqrt{2}}\left[\sum_j \psi_j\,|\phi_j\rangle\left(|0\rangle + e^{-iE_j\tau}\,|1\rangle\right)\right], \quad \text{(B11)}$$

which we now use to calculate the density matrix of the ancilla qubit:

$$\rho_{\text{ancilla}} = \text{Tr}_{\text{nonancilla}}\left(|\zeta\rangle\,\langle\zeta|\right)$$

$$= \frac{1}{2}\sum_{j,m}\text{Tr}_{\text{nonancilla}}\left\{\psi_j\,\psi_m^*\underbrace{\left[|\phi_j\rangle\,\langle\phi_m|\right]}_{\delta_{j,m}}\right.$$

$$\left.\times\,\left[|0\rangle + e^{-iE_j\tau}\,|1\rangle\right]\left[\langle 0| + e^{iE_m\tau}\,\langle 1|\right]\right\} \quad \text{(B12)}$$

$$= \sum_j \frac{|\psi_j|^2}{2}\left[|0\rangle + e^{-iE_j\tau}\,|1\rangle\right]\left[\langle 0| + e^{iE_j\tau}\,\langle 1|\right]$$

$$= \sum_j \frac{|\psi_j|^2}{2}\begin{pmatrix}1 & e^{iE_j\tau}\\ e^{-iE_j\tau} & 1\end{pmatrix}. \quad \text{(B13)}$$

2. Entangled-ancillas protocol

Our goal is to determine the purity of the ancilla. In general, there is the relation that ρ is pure if and only if $\text{Tr}[\rho^2] = \lambda_1^2 + \lambda_2^2 = 1$ for density matrices, where λ_1 and λ_2 are the eigenvalues of ρ. We write the density matrix and its square as

$$\rho_{\text{ancilla}} = \begin{pmatrix}a & b\\ c & d\end{pmatrix} \quad \text{and} \quad \rho^2_{\text{ancilla}} = \begin{pmatrix}a^2+bc & \cdot\\ \cdot & bc+d^2\end{pmatrix}, \quad \text{(B14)}$$

where matrix elements irrelevant to our protocol are denoted with a dot. With the Bell state

$$|\Phi^-\rangle = \frac{1}{\sqrt{2}}\left(|00\rangle - |11\rangle\right), \quad \text{(B15)}$$

we construct the Bell-measurement operator

$$|\Phi^-\rangle\,\langle\Phi^-| = \frac{1}{2}\begin{pmatrix}1 & 0 & 0 & -1\\ 0 & 0 & 0 & 0\\ 0 & 0 & 0 & 0\\ -1 & 0 & 0 & 1\end{pmatrix}. \quad \text{(B16)}$$

The diagonal matrix elements of ρ^2_{ancilla} may then be attained by considering a composite system where the second system features a controlled backward time evolution (implementable by changing the sign of H). Then, the density matrix of the ancilla of the second system effectively corresponds to the transpose of the density matrix of the first ancilla $\rho_{\text{ancilla2}} = \rho^T_{\text{ancilla1}}$. Using Eq. (B13), the

composite system then gives

$$\rho_{\text{ancilla1}} \otimes \rho_{\text{ancilla2}} = \rho_{\text{ancilla1}} \otimes \rho^T_{\text{ancilla1}} \tag{B17}$$

$$= \begin{pmatrix} a^2 & \cdot & \cdot & bc \\ \cdot & \cdot & \cdot & \cdot \\ \cdot & \cdot & \cdot & \cdot \\ bc & \cdot & \cdot & d^2 \end{pmatrix} = \frac{1}{4} \begin{pmatrix} 1 & \cdot & \cdot & |\alpha|^2 \\ \cdot & \cdot & \cdot & \cdot \\ \cdot & \cdot & \cdot & \cdot \\ |\alpha|^2 & \cdot & \cdot & 1 \end{pmatrix}. \tag{B18}$$

If $|\psi\rangle$ is in an eigenstate, the density matrix of the ancilla ρ_{ancilla} is pure and the expectation of the $|\Phi^-\rangle$ measurement is

$$\langle \rho_{\text{ancilla1}} \otimes \rho_{\text{ancilla2}} \rangle_{|\Phi^-\rangle} = \frac{1}{4}(1 - |\alpha|^2) = 0. \tag{B19}$$

3. Choosing suitable time values in the ancilla protocol

We argue that a measure for the eigenstate closeness is given by

$$\langle \psi | \psi_{\text{evo}} \rangle = \langle \sigma_x - i\sigma_y \rangle_{\text{ancilla}} = \sum_j |\psi_j|^2 e^{-iE_j \tau} =: \alpha, \tag{B20}$$

using the one-ancilla protocol. For suitable τ, $|\psi_{\text{evo}}\rangle$ is an eigenstate of the fixed Hamiltonian H only if $|\alpha| = 1$. The time τ needs to be chosen so that the complex summands of α with nonvanishing amplitude do not have approximately equal phases. In this unlikely case of matching phases, we would see constructive interference so that $\alpha = 1$ could be true even if $|\psi_{\text{evo}}\rangle$ is not an eigenstate. Visualizing the summands of α on a complex plane (Fig. 18), this becomes rather intuitive. The choice for τ is related to the spectrum of H. It is reasonable to assume and confirmed in our simulations that a quantum state in our algorithm has the largest overlap with the ground state. As transitions to high-energy excited states are extremely rare, for this argument we assume that the overlap with the first excited state is the only other nonvanishing overlap. Then, we simply have

$$\alpha = |\psi_0|^2 e^{-iE_0\tau} + |\psi_1|^2 e^{-iE_1\tau}. \tag{B21}$$

In the case of destructive interference,

$$|\alpha| = \min_\tau |\alpha(\tau)|, \tag{B22}$$

which corresponds to

$$e^{-iE_0\tau} + e^{-iE_1\tau} \stackrel{!}{=} 0 \Leftrightarrow \tau(E_1 - E_0) = \pi(2k+1) \tag{B23}$$

$$\Leftrightarrow \tau = \frac{\pi}{\Delta}(2k+1), \tag{B24}$$

where $k \in \mathbb{Z}$ and $\Delta = E_1 - E_0$. An arbitrary τ would correspond to choosing an $l \in \mathbb{Z}$ in $\tau = \pi l/\Delta$ at random. For

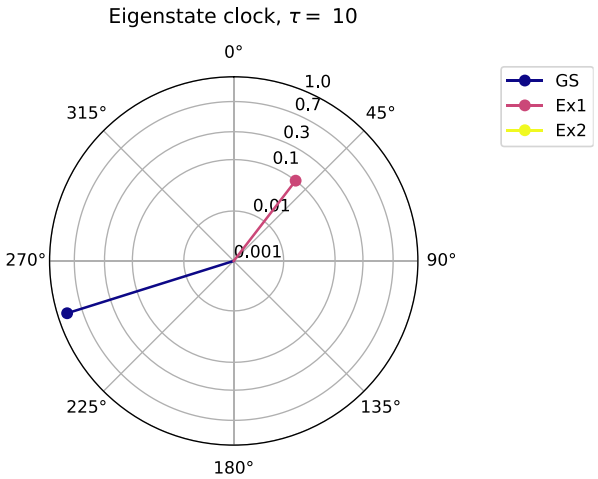

FIG. 18. The eigenstate clock for a second larger value of $\tau = 10$. For τ=1, the summand corresponding to the ground state and the summand corresponding to the first excited state lie quite closely together in phase, which leads to problematic constructive interference (Fig. 4). However, as the pointers rotate with their respective eigenenergies for changing τ, they are well separated for $\tau = 10$. Then, we find destructive interference in the summation, which is necessary for the explanatory power of the protocol. Note that in this instance, the summands corresponding to higher excited eigenstates are very small and not visible.

$l \gg 1$, the probability of choosing an odd value of l is approximately 1/2. Therefore, by testing several random values of $\tau \in O(\Delta^{-1})$, it is possible to deduce information about the system—whether it is in a mixed state or an eigenstate—with high confidence.

4. Bound for the single-ancilla protocol

We extend the discussion about suitable values of τ. As argued above, an answer is generally dependent on the spectral properties of H, which are not available *a priori*.

We provide a bound for the single-ancilla method without any knowledge about the spectrum of H or the populations of the different eigenstates. A side effect of this generality is that the bound is not tight. This is because in a realistic setting of a (quasi)adiabatic evolution, the eigenstate populations of higher excited states are expected to be very small.

We consider the expectation value [56] of $\alpha(\tau)$:

$$\mathbb{E}_{\tau \sim \text{unif. dist. in } [0,K]}[|\alpha(\tau)|^2] \tag{B25}$$

$$= \frac{1}{K}\int_0^K |\alpha(\tau)|^2 d\tau \tag{B26}$$

$$= \frac{1}{K}\int_0^K \sum_{i,j} |\psi_i|^2 |\psi_j|^2 e^{-iE_i\tau} e^{-iE_j\tau} d\tau \tag{B27}$$

$$= \sum_{i,j} |\psi_i|^2 |\psi_j|^2 \text{sinc}[(E_i - E_j)K]. \tag{B28}$$

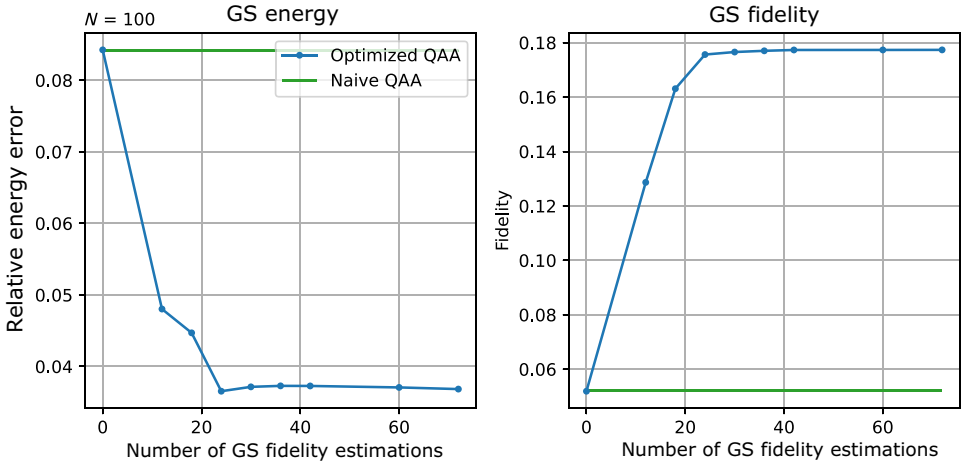

FIG. 19. The number of iterations required for this explicit instance. The optimizer algorithm is L-BFGS-B without any further adjustments. Very good results are already obtained after three iterations and fewer than 25 ground-state overlap evaluations. The data correspond to the first eight iterations of an instance of the black-box optimizer with five chunks for fixed total time $T = 1$ and $N = 100$.

In the limit of large K, we obtain

$$\lim_{K\to\infty} \mathbb{E}_{\tau\sim \text{unif. dist. in } [0,K]}[|\alpha(\tau)|^2] = \sum_i |\psi_i|^4 =: E^2, \tag{B29}$$

where the spectral dependence has entirely averaged out. Such an E^2 corresponds to what one would observe in the laboratory. We note that $|\psi_0|^2$ is the ground-state overlap of $|\psi\rangle$. As $|\psi\rangle$ is normalized, we can write

$$|\psi_i|^2 \le 1 - |\psi_0|^2 \quad \forall i > 0, \tag{B30}$$

i.e., for all i that do not correspond to the ground state. Then, multiplying by $|\psi_i|^2_{i>0}$ yields

$$|\psi_i|^4 \le \left(1 - |\psi_0|^2\right)|\psi_i|^2 \quad \forall i > 0. \tag{B31}$$

As the latter inequality holds for all $i > 0$, we obtain

$$\sum_{i=1} |\psi_i|^4 \le \left(1 - |\psi_0|^2\right)\sum_{i=1} |\psi_i|^2 = \left(1 - |\psi_0|^2\right)^2. \tag{B32}$$

For the expectation value E^2, we can now write down the inequality

$$E^2 = |\psi_0|^4 + \sum_{i=1} |\psi_i|^4 \le |\psi_0|^4 + \left(1 - |\psi_0|^2\right)^2. \tag{B33}$$

Solving for $|\psi_0|^2$, we obtain

$$|\psi_0|^2 \ge \frac{1}{2} + \frac{1}{2}\sqrt{2E^2 - 1}, \quad \text{or} \quad |\psi_0|^2 \le \frac{1}{2} - \frac{1}{2}\sqrt{2E^2 - 1}. \tag{B34}$$

So far, we have not made any assumptions about the populations. Letting the ground-state population $|\psi_0|^2$ be the largest of the eigenstate populations, we have

$$|\psi_0|^2 \ge \frac{1}{2} + \frac{1}{2}\sqrt{2E^2 - 1} \tag{B35}$$

as a lower bound for $|\psi_0|^2$ for $E^2 \ge 1/2$. Also, Eq. (B34) implies that in this case the smaller ground-state populations are therefore upper bounded as

$$|\psi_i|^2 \le \frac{1}{2} - \frac{1}{2}\sqrt{2E^2 - 1} \quad \forall i > 0. \tag{B36}$$

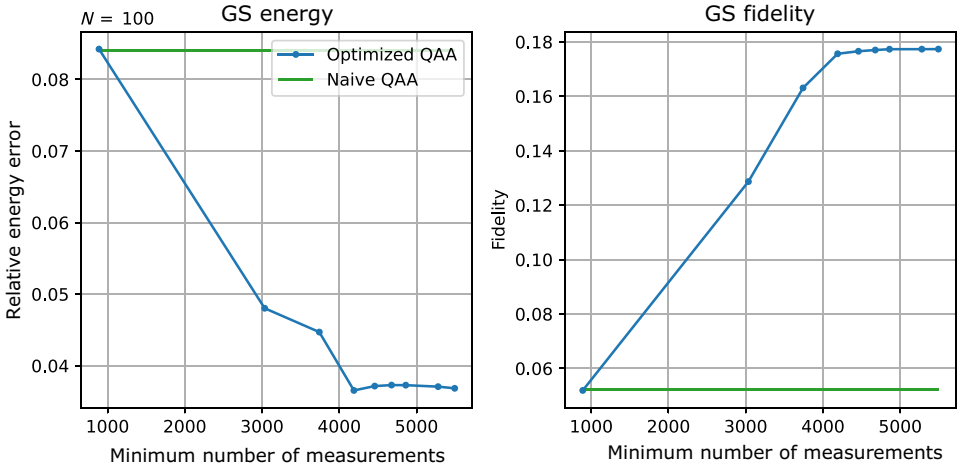

FIG. 20. The number of measurements for this explicit instance obtained using the Chernoff-Hoeffding inequality and the assumptions mentioned in the main text. For a total of a few thousand measurements, the end result of the adiabatic evolution is already improved significantly. The data correspond to the first eight iterations of an instance of the black-box optimizer with five chunks for fixed total time $T = 1$ and $N = 100$.

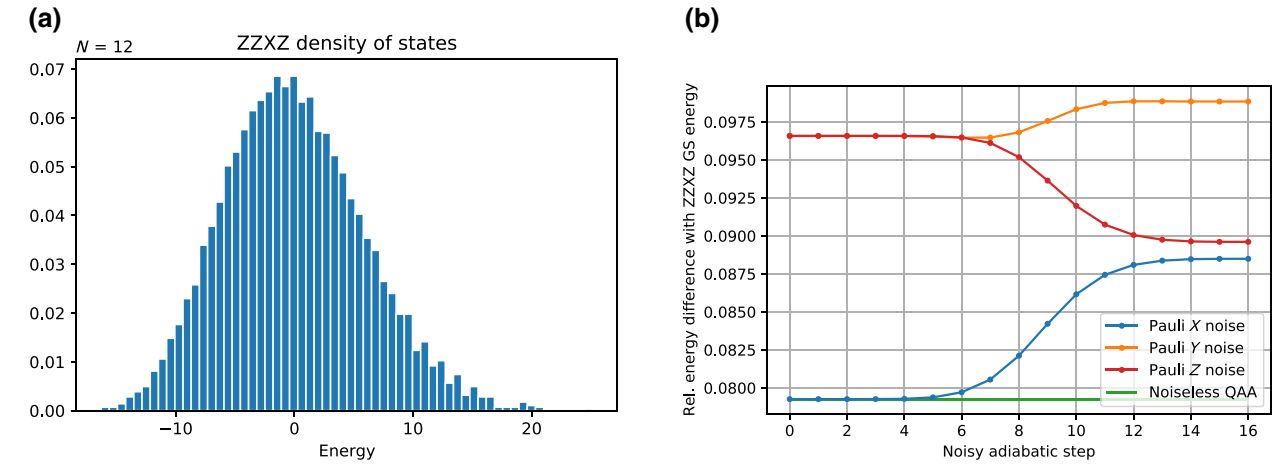

FIG. 21. Further plots on the robustness of the adiabatic evolution. (a) The energy density of states of the ZZXZ model for $N = 12$. Low-energy spectral lines are rare for physical instances. (b) The relative energy difference with the ZZXZ ground state, obtained using DMRG methods for adiabatic ground-state preparation. The total time is fixed to $T = 1$, corresponding to 16 discrete adiabatic steps. Pauli noise is applied either before the first unitary (step 0) or after each unitary to the center qubit of the spin chain. We observe that there is no qualitative difference regarding the position in the adiabatic path at which noise occurs. Note that for a σ^x noise gate, there is no difference in the energy at the beginning of the adiabatic path because the initial Hamiltonian H_0 commutes with σ^x.

For $E^2 < 1/2$, no nontrivial bound for $|\psi_0|^2$ (apart from $|\psi_0|^2 \in [0, 1]$) can be given in the limit of very large K (with this approach).

APPENDIX C: PLOTS ON THE NUMBER OF MEASUREMENTS AND NOISE

We include plots showing the number of ground-state overlaps for an instance of the black-box algorithm for $N = 100$ and five chunks. Also, we present an estimate of the number of measurements needed using the Chernoff-Hoeffding inequality (Fig. 20). For a discussion of the inherent robustness of adiabatic algorithm, we show the energy density of states for $N = 12$ for the ZZXZ model [Fig. 21(a)] and an analysis of the relative energy error due to a noisy gate at different positions in the adiabatic evolution [Fig. 21(b)].

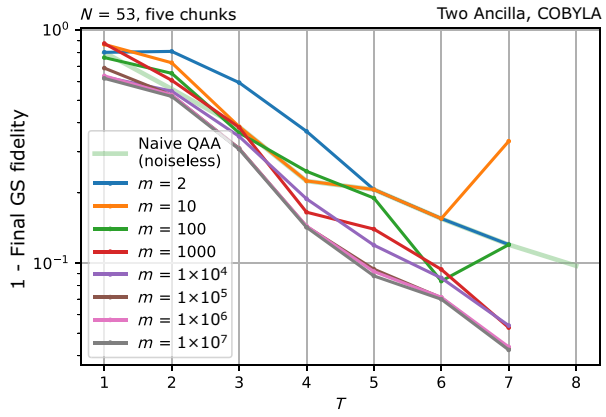

FIG. 22. The simulation of shot noise in the black-box algorithm for $N = 53$ and $J = 1$. Here, the two-ancilla method is used. The number of measurements taken for every ground-state overlap estimation is given by m. Note that no extra noise is applied during the circuit. COBYLA is used as the classical optimizer. For $m > 10^3$, the results begin to converge and the shot noise is sufficiently small.

[1] J. Preskill, Quantum computing in the NISQ era and beyond, Quantum **2**, 79 (2018).
[2] F. Arute, K. Arya, R. Babbush, D. Bacon, J. C. Bardin, R. Barends, R. Biswas, S. Boixo, F. G. Brandao, and D. A. Buell *et al.*, Quantum supremacy using a programmable superconducting processor, Nature **574**, 505 (2019).
[3] H.-S. Zhong, H. Wang, Y.-H. Deng, M.-C. Chen, L.-C. Peng, Y.-H. Luo, J. Qin, D. Wu, X. Ding, and Y. Hu *et al.*, Quantum computational advantage using photons, Science **370**, 1460 (2020).
[4] G. Wendin, Quantum information processing with superconducting circuits: A review, Rep. Prog. Phys. **80**, 106001 (2017).
[5] J. I. Cirac and P. Zoller, Goals and opportunities in quantum simulation, Nat. Phys. **8**, 264 (2012).
[6] C. Gross and I. Bloch, Quantum simulations with ultracold atoms in optical lattices, Science **357**, 995 (2017).
[7] J. Kempe, A. Kitaev, and O. Regev, The complexity of the local Hamiltonian problem, SIAM J. Comput. **35**, 1070 (2006).
[8] E. Farhi, J. Goldstone, S. Gutmann, and M. Sipser, Quantum computation by adiabatic evolution, arXiv preprint arXiv:quant-ph/0001106 (2000).
[9] A. Messiah, *Quantum Mechanics: Volume II* (North-Holland Publishing Company, Amsterdam, 1962).

[10] M. H. S. Amin, Consistency of the Adiabatic Theorem, Phys. Rev. Lett. **102**, 220401 (2009).

[11] S. Jansen, M.-B. Ruskai, and R. Seiler, Bounds for the adiabatic approximation with applications to quantum computation, J. Math. Phys. **48**, 102111 (2007).

[12] A. Elgart and G. A. Hagedorn, A note on the switching adiabatic theorem, J. Math. Phys. **53**, 102202 (2012).

[13] D. Guéry-Odelin, A. Ruschhaupt, A. Kiely, E. Torrontegui, S. Martínez-Garaot, and J. G. Muga, Shortcuts to adiabaticity: Concepts, methods, and applications, Rev. Mod. Phys. **91**, 045001 (2019).

[14] T. Albash and D. A. Lidar, Adiabatic quantum computation, Rev. Mod. Phys. **90**, 015002 (2018).

[15] J. Roland and N. J. Cerf, Quantum search by local adiabatic evolution, Phys. Rev. A **65**, 042308 (2002).

[16] A. T. Rezakhani, W.-J. Kuo, A. Hamma, D. A. Lidar, and P. Zanardi, Quantum Adiabatic Brachistochrone, Phys. Rev. Lett. **103**, 080502 (2009).

[17] E. Farhi, J. Goldstone, and S. Gutmann, A quantum approximate optimization algorithm, arXiv preprint arXiv:1411.4028 (2014).

[18] S. Wang, E. Fontana, M. Cerezo, K. Sharma, A. Sone, L. Cincio, and P. J. Coles, Noise-induced barren plateaus in variational quantum algorithms, Nat. Commun. **12**, 1 (2021).

[19] D. Stilck França and R. Garcia-Patron, Limitations of optimization algorithms on noisy quantum devices, Nat. Phys. **17**, 1221 (2021).

[20] M. Cerezo, A. Arrasmith, R. Babbush, S. C. Benjamin, S. Endo, K. Fujii, J. R. McClean, K. Mitarai, X. Yuan, and L. Cincio *et al.*, Variational quantum algorithms, Nat. Rev. Phys. **3**, 625 (2021).

[21] L. Bittel and M. Kliesch, Training Variational Quantum Algorithms is NP-Hard, Phys. Rev. Lett. **127**, 120502 (2021).

[22] M. A. Nielsen and I. L. Chuang, *Quantum Computation and Quantum Information (10th Anniversary edition)* (Cambridge University Press, Cambridge, UK, 2016).

[23] Y. Chen and T.-C. Wei, Quantum algorithm for spectral projection by measuring an ancilla iteratively, Phys. Rev. A **101**, 032339 (2020).

[24] P. Magnard, S. Storz, P. Kurpiers, J. Schär, F. Marxer, J. Lütolf, T. Walter, J.-C. Besse, M. Gabureac, and K. Reuer *et al.*, Microwave Quantum Link between Superconducting Circuits Housed in Spatially Separated Cryogenic Systems, Phys. Rev. Lett. **125**, 260502 (2020).

[25] Y. Matsuzaki, H. Hakoshima, K. Sugisaki, Y. Seki, and S. Kawabata, Direct estimation of the energy gap between the ground state and excited state with quantum annealing, Jpn. J. Appl. Phys. **60**, SBBI02 (2021).

[26] See the Supplemental Material at http://link.aps.org/supplemental/10.1103/PRXQuantum.3.020347 for a description of the QAA and QAOA, details on the numerical simulation techniques and notes on Bayesian inference in hypothesis testing, which also includes Refs. [57–72].

[27] The state $|+\rangle$ is an eigenvector of the Pauli matrix σ^x and is defined as $|+\rangle = (|0\rangle + |1\rangle)/\sqrt{2}$, where $|0\rangle$ and $|1\rangle$ are the computational-basis states.

[28] R. Santagati, J. Wang, A. A. Gentile, S. Paesani, N. Wiebe, J. R. McClean, S. Morley-Short, P. J. Shadbolt, D. Bonneau, and J. W. Silverstone *et al.*, Witnessing eigenstates for quantum simulation of Hamiltonian spectra, Sci. Adv. **4**, eaap9646 (2018).

[29] T. E. O'Brien, S. Polla, N. C. Rubin, W. J. Huggins, S. McArdle, S. Boixo, J. R. McClean, and R. Babbush, Error mitigation via verified phase estimation, PRX Quantum **2**, 020317 (2021).

[30] K. Boothby, P. Bunyk, J. Raymond, and A. Roy, Next-generation topology of D-Wave quantum processors, arXiv preprint arXiv:2003.00133 (2020).

[31] R. H. Byrd, P. Lu, J. Nocedal, and C. Zhu, A limited memory algorithm for bound constrained optimization, SIAM J. Sci. Comput. **16**, 1190 (1995).

[32] J. A. Nelder and R. Mead, A simplex method for function minimization, Comput. J. **7**, 308 (1965).

[33] J. I. Cirac, D. Perez-Garcia, N. Schuch, and F. Verstraete, Matrix product states and projected entangled pair states: Concepts, symmetries, theorems, Rev. Mod. Phys. **93**, 045003 (2021).

[34] The Pauli matrices are defined as $\sigma_x = \left(\begin{smallmatrix} 0 & 1 \\ 1 & 0 \end{smallmatrix}\right)$, $\sigma_y = \left(\begin{smallmatrix} 0 & -i \\ i & 0 \end{smallmatrix}\right)$ and $\sigma_z = \left(\begin{smallmatrix} 1 & 0 \\ 0 & -1 \end{smallmatrix}\right)$.

[35] A. A. Ovchinnikov, D. V. Dmitriev, V. Y. Krivnov, and V. O. Cheranovskii, Antiferromagnetic ising chain in a mixed transverse and longitudinal magnetic field, Phys. Rev. B **68**, 214406 (2003).

[36] M. Novotny and D. Landau, Zero temperature phase diagram for the $d = 1$ quantum ising antiferromagnet, J. Magn. Magn. Mater. **54**, 685 (1986).

[37] J. Wurtz and A. Polkovnikov, Emergent conservation laws and nonthermal states in the mixed-field ising model, Phys. Rev. B **101**, 195138 (2020).

[38] A. Benseny and K. Mølmer, Adiabatic theorem revisited: The unexpectedly good performance of adiabatic passage, Phys. Rev. A **103**, 062215 (2021).

[39] L. Zhou, S.-T. Wang, S. Choi, H. Pichler, and M. D. Lukin, Quantum Approximate Optimization Algorithm: Performance, Mechanism, and Implementation on Near-Term Devices, Phys. Rev. X **10**, 021067 (2020).

[40] W. Hoeffding, in *The Collected Works of Wassily Hoeffding* (Springer, 1994), p. 409.

[41] Y. Zhou, E. M. Stoudenmire, and X. Waintal, What Limits the Simulation of Quantum Computers?, Phys. Rev. X **10**, 041038 (2020).

[42] A. M. Childs, E. Farhi, and J. Preskill, Robustness of adiabatic quantum computation, Phys. Rev. A **65**, 012322 (2001).

[43] M. J. Powell, in *Numerical Analysis* (Springer, 1978), p. 144.

[44] S. Lu, M. C. Bañuls, and J. I. Cirac, Algorithms for quantum simulation at finite energies, PRX Quantum **2**, 020321 (2021).

[45] E. Urban, T. A. Johnson, T. Henage, L. Isenhower, D. Yavuz, T. Walker, and M. Saffman, Observation of Rydberg blockade between two atoms, Nat. Phys. **5**, 110 (2009).

[46] G. Rigolin, G. Ortiz, and V. H. Ponce, Beyond the quantum adiabatic approximation: Adiabatic perturbation theory, Phys. Rev. A **78**, 052508 (2008).

[47] J. Lin, Z. Y. Lai, and X. Li, Quantum adiabatic algorithm design using reinforcement learning, Phys. Rev. A **101**, 052327 (2020).
[48] X. Bonet-Monroig, R. Babbush, and T. E. O'Brien, Nearly Optimal Measurement Scheduling for Partial Tomography of Quantum States, Phys. Rev. X **10**, 031064 (2020).
[49] B. Koczor, Exponential Error Suppression for Near-Term Quantum Devices, Phys. Rev. X **11**, 031057 (2021).
[50] W. J. Huggins, S. McArdle, T. E. O'Brien, J. Lee, N. C. Rubin, S. Boixo, K. B. Whaley, R. Babbush, and J. R. McClean, Virtual Distillation for Quantum Error Mitigation, Phys. Rev. X **11**, 041036 (2021).
[51] S. Boixo, E. Knill, and R. D. Somma, Eigenpath traversal by phase randomization, Quantum Inf. Comput. **9**, 833 (2009).
[52] S. Ebadi, A. Keesling, M. Cain, T. T. Wang, H. Levine, D. Bluvstein, G. Semeghini, A. Omran, J.-G. Liu, R. Samajdar *et al.*, Quantum optimization of maximum independent set using Rydberg atom arrays, Science (2022).
[53] L. D. Landau, Zur Theorie der Energieübertragung II, Z. Sowjetunion **2**, 46 (1932).
[54] C. Zener, Non-adiabatic crossing of energy levels, Proc. R. Soc. London. Ser. A, Containing Papers Math. Phys. Character **137**, 696 (1932).
[55] C. De Grandi and A. Polkovnikov, in *Quantum Quenching, Annealing and Computation* (Springer, 2010), p. 75.
[56] In writing the expectation value, we make use of the (unnormalized) sinc function, which is defined as $\mathrm{sinc}(x) := \sin(x)/x$.
[57] M. C. Banuls, R. Orús, J. I. Latorre, A. Pérez, and P. Ruiz-Femenia, Simulation of many-qubit quantum computation with matrix product states, Phys. Rev. A **73**, 022344 (2006).
[58] N. Hatano and M. Suzuki, in *Quantum Annealing and Other Optimization Methods* (Springer, 2005), p. 37.
[59] U. Schollwöck, The density-matrix renormalization group in the age of matrix product states, Ann. Phys. (NY) **326**, 96 (2011).
[60] M. C. Bañuls, K. Cichy, J. I. Cirac, and K. Jansen, The mass spectrum of the Schwinger model with matrix product states, J. High Energy Phys. **2013**, 158 (2013).
[61] J. Hauschild and F. Pollmann, Efficient numerical simulations with Tensor Networks: Tensor Network PYTHON (TeNPy), SciPost Phys. Lect. Notes **5** (2018).
[62] D. Chruscinski and A. Jamiolkowski, *Geometric Phases in Classical and Quantum Mechanics* (Springer Science & Business Media, New York, 2004), Vol. 36.
[63] M. V. Berry, Quantal phase factors accompanying adiabatic changes, Proc. R. Soc. London. A. Math. Phys. Sci. **392**, 45 (1984).
[64] A. Kay, Tutorial on the QUANTIKZ package, arXiv preprint arXiv:1809.03842 (2018).
[65] M. B. Hastings, An area law for one-dimensional quantum systems, J. Stat. Mech.: Theory Exp. **2007**, P08024 (2007).
[66] F. Verstraete and J. I. Cirac, Matrix product states represent ground states faithfully, Phys. Rev. B **73**, 094423 (2006).
[67] G. Vidal, Efficient Simulation of One-Dimensional Quantum Many-Body Systems, Phys. Rev. Lett. **93**, 040502 (2004).
[68] S. Paeckel, T. Köhler, A. Swoboda, S. R. Manmana, U. Schollwöck, and C. Hubig, Time-evolution methods for matrix-product states, Ann. Phys. (NY) **411**, 167998 (2019).
[69] M. Kormos, M. Collura, G. Takács, and P. Calabrese, Real-time confinement following a quantum quench to a non-integrable model, Nat. Phys. **13**, 246 (2017).
[70] V. V. Shende, I. L. Markov, and S. S. Bullock, Minimal universal two-qubit controlled-NOT-based circuits, Phys. Rev. A **69**, 062321 (2004).
[71] A. Barenco, C. H. Bennett, R. Cleve, D. P. DiVincenzo, N. Margolus, P. Shor, T. Sleator, J. A. Smolin, and H. Weinfurter, Elementary gates for quantum computation, Phys. Rev. A **52**, 3457 (1995).
[72] G. Gundersen, Bayesian inference for beta-Bernoulli models (2020), accessed: 12 February 2021.